JOINT INSTITUTE FOR LABORATORY ASTROPHYSICS

UNIVERSITY OF COLORADO
BOULDER, COLORADO 80309

UNIVERSITY OF COLORADO

NATIONAL BUREAU OF STANDARDS

(12)
NW

LEVEL II

SEMIANNUAL REPORT

RESEARCH IN LASER PROCESSES

Research Sponsored by
Advanced Research Projects Agency

and

Office of Naval Research

ARPA Order No. 2683, Amendment 8
Program Code No. 8E20
Contractor: University of Colorado
Effective Date of Contract: 1 July 1975
Contract Expiration Date: 15 May 1980
Amount of Contract: $580,000
Period Covered: 1 February 1979 to
31 July 1979

Contract No. N00014-76-C0123
Principal Investigators:
A.V. Phelps
Telephone: (303) 492-7850
A.C. Gallagher
Telephone: (303) 492-7841
Scientific Officer: Director,
Physics Program, ONR
Short Title of Work: Laser Processes

15 April 1980

Cable Address: JILA

Telephone Number: 492-7789

Unclassified

SECURITY CLASSIFICATION OF THIS PAGE (When Data Entered)

REPORT DOCUMENTATION PAGE

READ INSTRUCTIONS BEFORE COMPLETING FORM

1. REPORT NUMBER: None

2. GOVT ACCESSION NO.

3. RECIPIENT'S CATALOG NUMBER

4. TITLE (and Subtitle): Semiannual Report - Research in Laser Processes

5. TYPE OF REPORT & PERIOD COVERED: Semiannual Report, 1 Feb [redacted]-31 Jul [redacted]79

6. PERFORMING ORG. REPORT NUMBER

7. AUTHOR(s): A. V. Phelps [redacted] A. C. Gallagher

8. CONTRACT OR GRANT NUMBER(s): N00014-76-C-0123; ARPA Order-2683

9. PERFORMING ORGANIZATION NAME AND ADDRESS
University of Colorado
Joint Institute for Laboratory Astrophysics
Boulder, CO 80309

10. PROGRAM ELEMENT, PROJECT, TASK AREA & WORK UNIT NUMBERS
NR 393-506/3-21-79, Code 421
ARPA Ord. No. 2683, Amd. 8, Prog. Cd. 8E20

11. CONTROLLING OFFICE NAME AND ADDRESS
Office of Naval Research
Department of the Navy
800 North Quincy Street, Arlington, VA 22217

12. REPORT DATE: 15 Apr [redacted]80

13. NUMBER OF PAGES: 48

14. MONITORING AGENCY NAME & ADDRESS (if different from Controlling Office)

15. SECURITY CLASS. (of this report): Unclassified

15a. DECLASSIFICATION/DOWNGRADING SCHEDULE

16. DISTRIBUTION STATEMENT (of this Report)

Distribution unlimited

17. DISTRIBUTION STATEMENT (of the abstract entered in Block 20, if different from Report)

18. SUPPLEMENTARY NOTES

19. KEY WORDS (Continue on reverse side if necessary and identify by block number)

Laser, processes, sodium vapor, rare gas, electrical discharge, high pressure, molecules, metastables, neon, absorption, dye laser

20. ABSTRACT (Continue on reverse side if necessary and identify by block number)

A model has been completed of the NaXe discharges examined experimentally under this contract. This model includes the effects of electron excitation, deexcitation and ionization of excited Na atoms, as well as electron loss processes such as dissociative recombination with Na_2^+. By adopting apparently reasonable rate coefficients and reaction end products we are able to satisfactorily reproduce the measured steady-state densities of excited Na atoms. However, a serious and unexplained discrepancy is found in the energy (continued)

DD FORM 1 JAN 73 1473

Unclassified 192900

SECURITY CLASSIFICATION OF THIS PAGE (When Data Entered)

80 4 23 004

20. Abstract (continued)

balance for these discharges. By extrapolating these results to high Na densities we find what appears to be a region of sufficient optical gain at 700 nm for laser oscillation. Such a laser would require a short excitation pulse (~ 100 ns) and would have a low discharge impedance.

A new technique has been developed for the measurement of electron excitation rate coefficients for the metastable states of the rare gases. A multipass absorption cell and a single mode dye laser allow measurement of metastable densities as low as 10^6 atom/cm^3.

SEMIANNUAL REPORT

This Semiannual Report contains descriptions of work carried out under ONR Contract No. N00014-76-0123 and ARPA Order No. 2683-Amd. 8. It covers the period from 1 February 1979 to 31 July 1979. Section I is the Semiannual Report Summary, while Sections II-IV are more detailed descriptions of work carried out under the projects supported by this contract.

I. SEMIANNUAL REPORT SUMMARY

The projects being carried out under this contract are summarized below. More detailed discussions are given in Sections II-IV of this report.

(1) Metal Vapor-Rare Gas Discharges

The objective of this project is the evaluation of the potential of electrical discharges in high pressure metal vapor-rare gas mixtures for excitation of high power, high efficiency lasers operating at near visible wavelengths. Our work has provided stimulated emission coefficients for several metal vapor-rare gas excimers at visible or near visible wavelengths and has shown that electrical discharges with sufficiently high electron temperatures (>0.5 eV) are an efficient way to produce these excimers. Our recent experiments under this contract have shown that the effective electron temperature in high power discharges in Na-Xe mixtures with Na densities between 10^{15} and 10^{16} cm^{-3} is too low to yield useful gain on the Na-Xe excimer transition.

During this report period we have completed work on a detailed model of the high power discharges in Na-Xe mixtures which we have examined experimentally under this contract. The objective of this theoretical investigation is to determine the dominant electronic and atomic collisional processes that control the optical and electrical properties of these discharges. This information can then be used to predict and hopefully to improve the suitability of these discharges for high power laser applications.

High power (~10^8 W/ℓ) discharges in metal-doped Xe are modeled for typical metal atom densities of 10^{15}-10^{17} cm^{-3} and Xe densities of ~10^{20} cm^{-3} and electron densities of 10^{14}-10^{17} cm^{-3} as appropriate for proposed excimer lasers. Na is used as a prototype species, while its properties are varied to indicate some of the changes that could result from the use of different metals. The model includes sixteen excited levels of Na, three ions, and

the excimer levels of NaXe and Na_2. The degree of ionization is determined by collisional multistep excitation and ionization of excited atoms vs dissociative recombination of electrons with Na_2^+. Steady-state conditions in the positive column are calculated for typical gas temperatures of ~0.06 eV and electron temperatures T_e of 0.3-0.5 eV. The Na population distribution is largely Boltzmann at the electron temperature and the electron density is close to the Saha equilibrium value except at low electron temperatures and very high extracted laser powers. Useful gain and extracted powers of ~10 MW/cm^3 are predicted for the higher T_e and Na densities, with the pulse width limited to $\sim 10^{-7}$ sec by gas heating. The model indicates that a metal which produces a deeply bound product state via dissociative recombination could yield a very efficient, high power laser or gain cell.

(2) Electron Excitation Rates in Metal Vapors

The objective of this new project is to determine effective rate coefficients for the electron excitation and deexcitation of excited mercury atoms for use in the modeling of the role of these excited atoms in electrically excited, high power lasers, e.g., mercury-halogen lasers. In order to minimize problems with chemical reactivity, these experiments are being carried out in mercury-rare gas mixtures. The electrical and optical properties of discharges in this mixture are being investigated under another contract. This work is a prerequisite to the rate coefficient determinations and is currently directed toward (a) absolute calibration of the optical detection system so as to allow more accurate determinations of the densities of the excited states of mercury and (b) installation of an auxiliary discharge so as to provide initiating electrons and so improve the stability of the main discharge. Once these discharges are operating stably and are characterized, the present investigation

will make use of laser perturbation techniques and fast transient analysis of the emitted radiation to obtain the desired rate coefficients. The fast transient digitizer and the N_2 pulsed dye laser for this experiment have been acquired and tested. This means that the desired measurements will not be made until near the end of this contract.

(3) Electron Excitation of Metastable Atoms and Molecules

During this report period we assembled and tested apparatus for measurement of electron excitation rate coefficients for the lower metastable and radiating states of neon. Electron excitation rate coefficients for the lower excited states of the rare gases are essential to the prediction and understanding of the efficiency and power output of electrical discharge excited, high power rare gas-halogen lasers. In particular, recent work at the Naval Research Laboratory has shown that the use of Ne as the principal rare gas results in significant improvements in rare gas-halogen laser performance. This result and the convenience of neon wavelengths led to our choice of neon for this demonstration experiment. Resources will not be available to extend these measurements to the other rare gases.

The technique being used for the measurement of the neon metastable and resonance state densities is that of the absorption of radiation in transitions from the metastable (or resonance) state to a more highly excited state. In order to eliminate the usual uncertainties in derived metastable densities caused by uncertainties in the spectral profile of the incident neon radiation, we have replaced the usual neon discharge source with a single mode dye laser, i.e., with a source whose spectral width is narrow compared to the absorption profile. The use of a narrow laser beam also allows us to use a multipass absorption cell and so bring the absorption signal up to levels well above the noise level of the system. This arrangement has been tested and measurements

will be made during the next report period.

II. METAL VAPOR-RARE GAS DISCHARGES

Drs. L. W. Schumann, A. Gallagher and A. V. Phelps

We have chosen to model the discharge excited Na-Xe excimer system because of the relatively large amount of collisional cross section data available for Na and because of the availability of experimental data for comparison with our theory. It is believed that many of the properties of these particular species are characteristic of other mixtures, as long as the ionization energy of the dopant is below the first excited state of the noble gas, and the electron affinity of the dopant is small enough that negative ion densities are insignificant. Much of this work was carried out earlier by R. Shuker.

Note that for completeness this discussion includes some results of the measurements on Tℓ-Xe discharges carried out under another contract (AFWL Agreement 78-036).

A. DETAILS OF THE MODEL

a) Discharge conditions

The pulsed discharges under consideration typically occur in Xe at densities of $[Xe] = 10^{19}$-10^{20} cm^{-3} doped with Na at densities of $[Na] = 10^{15}$-3×10^{17} cm^{-3}. The electron densities (n_e) are typically 10^{14}-10^{17} cm^{-3}, the electric field to total gas density ratios E/N are in the 10^{-18}-10^{-17} V cm^2 range, the electron temperature T_e is 0.3-0.5 eV, and the gas temperature T ≅ 800K, so that kT ≅ 0.07 eV. Here and throughout this paper electron temperatures are expressed in eV. Typical modeled discharge power densities are 10-10^4 MW/ℓ. It is assumed that quasi-steady-state discharges will be terminated before excessive (∿300°C) gas heating occurs. The present models thereby emphasize steady-state, constant gas temperature conditions. Results in Sec. IIB are obtained by integration of

nonlinear, time dependent rate equations, and in Sec. IID by use of a two-temperature approximation. The near-uniform cylindrical spatial character of the discharge under consideration is described in Ref. 1. Here we consider only a uniformly excited region in the positive column of the discharge. The fractional ionization in the discharges is high enough so that electron-electron collisions could be expected to largely Maxwellianize the electron energy distribution.[2] Thus, the calculations presented here utilize Maxwellian electron energy distributions and Na excited states up to an effective quantum number of 15.

b) Atomic states

An Na(3P)/Na(3S) fraction of ~0.05, which is equivalent to an ~0.5 eV excitation temperature, is desired for efficient laser action. (As another example, Tℓ(7S)/Tℓ($6P_{1/2}$) ≅ 0.02 equivalent to T_e ≅ 0.85 eV is desired for a Tℓ-Xe excimer laser.[3]) If this excitation temperature results from a balance between electron excitation and deexcitation of Na(3P), then an electron temperature T_e of ~0.5 eV is necessary. Electron collisions with Na(3P) atoms will then tend to produce a similar excitation temperature between Na(3P) and higher excited states. Radiation will lower the excited state populations, but at the electron densities in these discharges this is a minor effect. If the excited Na densities are characterized by an excitation temperature in this 0.5 eV range, then the electron collisional excitation and ionization rates out of excited levels increase with increasing excitation energy of the level. Thus, highly excited states must be considered in the ionization balance. We have included Na states with an effective principal quantum number n up to 15 in the present model, and we allow for the effect of still higher levels through the collisional rate coefficients assigned to this terminal n = 15 level.

The highly excited Na states are strongly mixed by electron collisions,

so that most of the population resides in the high angular momentum states. These states are very hydrogenic and very nearly degenerate at integral n values. Consequently we have simplified the level structure by grouping all states above 4P into 11 hydrogenic levels, n = 4 to 15, as shown in Figs. 1 and 2. This also allows the use of hydrogenic cross sections for electron collisions with the highly excited states. The rate coefficients for these collisions are obtained from the literature[3,4] and by scaling, and are shown in Fig. 3. The lowest excited states of Xe, i.e., a single Xe^*, and ionization ($e + Xe^* \rightleftarrows 2e + Xe^+$) are included in the model. In fact, the Xe^+ ions are rapidly converted into Xe_2^+ ions, which undergo dissociative recombination to form Xe^*. For the T_e considered here, the densities of Xe^+ and Xe^* are much lower than Na^+ and Na^*, and they do not significantly influence the kinetics.

c) Molecular species

The lower energy levels and ionic forms of Na, Na_2, and NaXe are shown in Fig. 2. The A-X band of the NaXe excimer is a broad continuum extending from the 590 nm Na resonance line to ~720 nm; the 700 nm region of this band is the most favorable region for excimer laser action.[5] The B state of NaXe, not shown in Fig. 2, is a repulsive state correlating asymptotically with Na(3P) and Xe($^1S_0$). The B-X band of NaXe extending from 560-590 nm is very weak and from thermodynamic arguments is not expected to exhibit net gain.[1] The $4S\Sigma$ state radiates a $4S\Sigma$-$X\Sigma$ band[6] which could have net gain in the present discharges if sufficiently high excitation temperatures are obtained. Higher levels of NaXe are not shown, but they are expected to exhibit a Rydberg-like shape, approximately paralleling the $NaXe^+$ potential.[7]

At the typical Na densities of 10^{15}-10^{-17} cm^{-3} under consideration, a few percent of the Na is bound as Na_2. The associated A-X (560-800 nm) and B-X (450-500 nm) bands of Na_2 can cause severe absorption, although the A-X band

may also be capable of yielding net gain in a discharge.[8] The radiative lifetimes of the Na_2 A and B states are about 10 nsec. The $A^1\Sigma_u^+$, $a^3\Pi_u$, and $X^1\Sigma_g^+$ states of Na_2 are strongly bound[9] so that the Xe induced collisional dissociation rate coefficient is very small. The relative populations of the A and a states are expected to be maintained in approximate statistical equilibrium and are represented in the model by an A' state. Since Na_2 molecules are depleted by electron induced dissociative excitation, the Na_2 states are expected to be present at much less than their equilibrium fractions. In order to evaluate this effect, the A' and X states of Na_2 are included in the calculation, although they are minor constituents.

The NaXe(A) state is bound by only a few kT, so that the Na(3P) and NaXe(A) densities are maintained at their gas temperature equilibrium ratio, typically 10% as molecules for [Xe] = 2.7×10^{20} cm^{-3}, by rapid association and dissociation, i.e., we assume equilibrium for the reaction

$$Na(3P) + 2Xe \leftrightarrow NaXe(A) + Xe \quad .$$

The dissociation rate per NaXe(A) molecule is about 10^{10} sec^{-1} at typical [Xe] = 10^{20} cm^{-3}, so that the equilibrium ratio of $[NaXe(A)]/[Na(3P)][Xe] = K_{eq}^A$ is maintained as long as the destruction of NaXe(A) as the result of deexcitation by stimulated emission and of dissociation and deexcitation by electrons is slower than 10^{10} sec^{-1}. This is expected to hold at the ratio $n_e/[Xe] < 10^{-3}$ and the incident optical intensities considered here. Vibrational and rotational excitation of NaXe A-state molecules by electrons is expected to be slow compared to vibrational and rotational relaxation by Xe so that these electron collisions can be ignored. The observation in Ref. 1 of a nearly thermal excimer band shape, corresponding to a vibrational temperature at the gas temperature T, also supports these expectations. In

the present calculation we therefore include only molecular states connecting to the Na(3P) states, with the implicit assumption that the equilibrium portion of this is in the form of NaXe A-state molecules. Thus all inelastic collision cross sections of electrons with the molecules are effectively assumed to be identical to those for the parent Na state.

The Na(3P) states radiate with a lifetime of 16 nsec while the NaXe A and B states have slightly longer and shorter radiative lifetimes, respectively. Therefore, the combined Na(3P) + NaXe(B) + NaXe(A) population radiates with an effective lifetime near 16 nsec. From the normalized emission spectrum of this composite population, and the absorption coefficient derived therefrom,[5] one finds about a 10% probability that a photon is emitted in an optically thin portion of the spectrum (for 0.2 cm escape distance and [Xe] ~ 10^{20} cm^{-3}), i.e., the effective radiative lifetime for this combined population is about 160 nsec. This effective radiative rate constant is not very sensitive to [Na] and it scales linearly with [Xe] for values below 10^{21} cm^{-3}. The stimulated emission coefficient at 700 nm is ~10^{-16} cm^2 per NaXe(A) molecule, and thus is ~10^{-17} cm^2 per total Na(3P) population (bound and free) at [Xe] = 10^{20} cm^{-3}. Some of the transitions from higher Na states to Na(3P) are also slightly optically thick, but as their radiative rates are much smaller than their electron collisional rates this is ignored in the calculations.

The $NaXe^+$ molecular ion is structurally an Na^+-Xe molecule, whose potential (Fig. 2) we take to have ~0.3 eV binding and R_e ~ 3.2 Å from experiments and theory.[7] (We have no information about T&Xe^+.) The fact that only one molecular ground state results from this interaction between closed shell ($^1S_0$) monomers has a profound effect on its collisional and optical properties. Thus $NaXe^+$ cannot absorb in the visible, and the highly excited states of Na^*-Xe will all nearly parallel the single Na^+-Xe potential.

The latter property yields the expectation that Xe collisions will not efficiently quench highly excited Na^* atoms or bound Na^*-Xe molecules and, as discussed further below, that dissociative recombination with $NaXe^+$ will have a small rate coefficient.[10] The reactions $Na^+ + 2Xe \rightleftarrows NaXe^+ + Xe$ will be very fast[7] at high [Xe], yielding a ratio of $[NaXe^+]/[Na^+][Xe]$ very close to the equilibrium ratio K_{eq}^+ at all n_e considered here. As discussed in Sec. IIB, the size of K_{eq}^+ is very important in determining the effective rate of electron recombination in the discharge.

The Na_2^+ molecular ion potentials, from Ref. 9, are shown in Fig. 2. Under the conditions considered below Na_2^+ is a minor constituent in the discharge, so that absorption by Na_2^+ (see Ref. 11) and emission from excited states of Na_2^+ are expected to be negligible. However, $e + Na_2^+ \rightarrow Na^* + Na$ is the dominant electron recombination mechanism in our model. Na_2^+ will be formed by the exchange reaction $Na + NaXe^+ \rightarrow Na_2^+ + Xe$. Due to the low [Na]/[Xe] ratio the equilibrium ratio of $[Na_2^+]/[NaXe^+]$ is typically on the order of 1; rapid dissociative recombination of Na_2^+ normally makes this ratio much smaller.

The highly excited states of Na are expected to have associated NaXe states with binding energies about equal to that of $NaXe^+$. If predissociation of lower excited states of NaXe occurs to form excited Na, the loss of $NaXe^*$ will cause a net downward flow of excitation in the molecular excited state ladder and produce departures of the Na^* populations from Boltzmann equilibrium in the same manner as dissociative recombination of electrons with $NaXe^+$. However, as discussed in Sec. IIB, the experimental lower excited state population data seem to show that departures from the Boltzmann plot are small.

d) Electrons

At the typical ionization fraction of interest to us, i.e., $n_e/[Xe] \sim 10^{-4}$, energy exchange by electron-electron collisions is much more rapid than energy loss by recoil of Xe. Inelastic and superelastic collisions with Na^* are largely in balance so that the net energy transfer rate between electrons and Na^* is much smaller than between free electrons. Therefore the electron energy distribution is expected to be very nearly Maxwellian at a temperature T_e. The range of validity of this assumption for the higher excited state densities is being investigated separately.[12]

e) Collision rate coefficients

The simplified model used considers the states shown in Fig. 1, plus Xe^*, Xe^+ and Xe_2^+. In addition to $Na_2(X)$, $Na_2(A)$, Na^+, $NaXe^+$, and Na_2^+, hydrogenic levels of Na from n = 4 to 15 and the 3S, 3P, 4S, 3D, and 4P levels of Na are included. Electron collision rate coefficients between n = 4 to 15 levels and for ionization of these levels are calculated from the hydrogenic cross sections of Johnson,[3] by integrating over the assumed Maxwellian energy distribution, and are shown in Fig. 3. Calculations by Moores et al[4] are used for cross sections within the five lower Na levels, and scaling and detailed balance arguments are used for rate coefficients between the five lower Na and the n = 4 to 15 levels. In order to account for the n > 15 levels that are neglected, we give the n = 15 level an ionization rate coefficient equal to about one third the rate for the n = 15 to n = 16 step. This is close to the effective multi-step ionization rate coefficient.[13] The n = 14 ionization rate coefficient is found by interpolation between the n = 13 and n = 15 values. Since the electron energy distribution is Maxwellian, all $i \rightarrow j$ rate coefficients, k_{ij}, are related by the thermodynamic ratio $k_{ij}/k_{ji} = (g_j/g_i)\exp[(E_i-E_j)/kT_e]$. The thermodynamic (Saha) equilibrium condition is also used to relate ionization and inverse

ionization rate coefficients. This condition is usually written as

$$\frac{n_e}{g_e}\frac{[Na^+]}{g_+} = \frac{[Na(n)]}{g_n}\left(\frac{2\pi mkT_e}{h^2}\right)^{3/2} \exp[-E_I(n)/kT_e] \quad , \qquad (1)$$

where $E_I(n)$ is the ionization potential of the n'th level. The statistical weights are $g_e = 2$ for the electrons and $g_+ = 1$ for Na^+. The g_n vary from 2 for the 3S level to $2n^2$ for the hydrogenic levels.

The only heavy particle collision rates entering the rate equations are those for $Na_2(X)$ and $Na_2(A')$ association and dissociation[8] (as noted above the NaXe(A)/Na(3P) ratio is assumed in equilibrium), i.e.,

$$Na(3S) + Na + Xe \rightleftarrows Na_2(X) + Xe + 0.5 \text{ eV} \quad ,$$

and

$$Na(3P) + Na + Xe \rightleftarrows Na_2(A') + Xe + 1 \text{ eV} \quad ,$$

and for the ion-molecule processes

$$Na^+ + 2Xe \rightleftarrows NaXe^+ + Xe + 0.3 \text{ eV} \quad ,$$

and

$$NaXe^+ + Na \rightleftarrows Na_2^+ + Xe + 0.7 \text{ eV} \quad .$$

We assume that all molecules are in an equilibrated vibrational and rotational distribution at T, and the ratio of forward to backward rate coefficients is given by equilibrium relations at the gas temperature T.

One of the most important processes controlling the behavior of these discharges, in which most of the ions are molecular and $T \ll T_e$, is dissociative recombination of electrons with the molecular ions. Dissociative recombination is generally described[14] in terms of a curve crossing of the dissociative diatomic state (AB^*) with the molecular ion state (AB^+). In homonuclear

diatomics such crossings always occur because symmetry considerations lead to repulsive as well as an attractive molecular-ion state; thus some of the Rydberg-like A_2^* states will parallel this repulsive state and cross the (attractive) A_2^+ state. This situation applies to Na_2^+ dissociative recombination, so that we expect it to have the typical large rate coefficient observed for the heavier inert gas diatomics,[15] e.g., $2 \times 10^{-7}\ (0.026/T_e)^{1/2}$ cm^3/sec. For $NaXe^+$, on the other hand, only one attractive state occurs and the Rydberg-like $NaXe^*$ states will not cross this ion state. The rate coefficient for $NaXe^+$ dissociative recombination is thereby expected[10] to be much smaller than the Na_2^+ value. Including $NaXe_n^+$ clusters does not modify this conclusion. For the same reasons associative ionization to form $NaXe^+$ is assumed not to occur. Consequently, we have taken $\alpha(NaXe^+) = 0$ in most of the calculations. Unless the rate coefficient for $Na^+ + Na + Xe \rightarrow Na_2^+ + Xe$ were usually large, e.g., 10^{-28} cm^3/sec^{-1}, the Na_2^+ is formed predominantly from $NaXe^+$ through the $NaXe^+ + Na \rightarrow Na_2^+ + Xe$ ion exchange process. Due to the low Na density this process is usually the rate limiting step that determines the electron-ion loss rate in the discharge. For this ion exchange rate coefficient k_a we use a Langevin rate coefficient, and believe that this should be fairly accurate. However, the final Na^* product state of the Na_2^+ dissociative recombination must be estimated by fitting the model to the experiments.

The curve-crossing model predicts that the final state products of Na_2^+ dissociative recombination ($Na_2^+ + e \rightarrow Na(n_R) + Na$) will be an atomic state bound by about 2.3 eV, the vertical dissociation energy of Na_2^+. This would apply to Na_2^+ in the ground vibrational state, whereas the same model would predict that an excited vibrational state would dissociate to less strongly bound Na^* states. Thus, we expect a distribution of final states, labeled by principal quantum numbers n_R, with the mean values of n_R increasing with Na_2^+

vibrational temperature. For convenience we often use a single n_R, representing the effective value of this distribution.

Destruction of excited Na in collisions with Na, by associative ionization to form $Na_2^+ + e$, occurs with a typical gas kinetic rate coefficient.[16] Due to the low Na density it is negligible compared to multistep ionization by electrons. Similarly, ion pair formation ($Na^* + Na \rightarrow Na^+ + Na^-$) is negligible.

We do not expect excitation and deexcitation of the highly excited Na states in collisions with Xe atoms to compete with electron excitation and deexcitation, since these Rydberg-like $NaXe^*$ potentials should be approximately parallel to the single $NaXe^+$ potential and do not provide the necessary curve crossings. Even in the case of the homonuclear system of H^* collisions with H atoms, theory[17] shows the electron collisions dominate for $[e]/[H] > 10^{-5}$. We have tested for the influence of a $n = 5 \rightarrow 4$ quenching rate coefficient of 3×10^{-10} cm^3/sec^{-1}, the maximum rate that appears feasible in the absence of long-range curve crossings,[18] and found it negligible under typical discharge conditions. Collisional deexcitation of higher states is expected to cause still smaller population changes, so no deexcitation by Xe is included in the calculations reported here.

The model described above is the basis for formulating a set of differential equations which describes the various processes occurring in the discharge and the time evolution of the species' densities and level populations. The rate equations are stiff differential equations and are solved numerically using a Gear package.[19]

B. RESULTS

The efficiency and pulse energy of lasers based on the discharges discussed in this report are greater if they can operate during the relatively long steady-state portion of the discharge. This is due to the energy initially

required to ionize a major fraction of the Na atoms. The data in Refs. 1 and 20, to which we will compare, also represent steady-state conditions. Consequently we will concentrate here on the calculated steady-state densities of the 17 Na states in the model, and of the ion and electron densities. The calculations were made for fixed electron temperatures. As expected, there is an exponential buildup of n_e from the assumed starting electron density of 10^{10} cm^{-3}, an increasing rate of ionization as n_e increases, and once n_e exceeds about 10^{14} cm^{-3}, convergence to the steady-state conditions within a few nanoseconds. In cases where the neutral Na density is severely depleted at steady state, the excited-state densities are larger during the rapid ionization transient than for steady-state conditions.

The excited state and ion densities in the steady-state positive column depend on T_e, n_R, and the effective dissociative recombination rate per Na^+ ion. The latter rate depends on the $[NaXe^+]/[Na^+]$ ratio, which is assumed in equilibrium at the gas temperature. Since Na_2^+ is formed by $NaXe^+ + Na \rightarrow Na_2^+ + Xe$, with rate coefficient k_a, the effective Na_2^+ dissociative recombination rate per Na^+ is proportional to $k_a [NaXe^+]$. The actual ratio $[NaXe^+]/[Na^+] = K_{eq}^+[Xe]$ is <0.5 at the $[Xe] < 4.5 \times 10^{19}$ considered in Ref. 1, and as a result the effective dissociative recombination rate is too small to significantly perturb the $[Na^*]$ and $[Na^+]$ densities, i.e., these densities relative to [Na] are very close to the Saha ratios at T_e, in agreement with the Na-Xe discharge data in Ref. 1. The laser gain which results from this limit is considered in Sec. IID.

In contrast to the Na-Xe case, the Tℓ-Xe discharge data of Ref. 20 does not fit the Saha relation for the higher n. This implies that more rapid dissociative recombination and thus larger values of $K_{eq}^+[Xe]$ and/or a much lower energy for the atomic lervel resulting from dissociative recombination. In order to investigate this type of behavior we have used all other cross sections as appropriate to Na and Xe, but increased K_{eq}^+ by a factor of 10-20,

corresponding to 0.45 eV rather than 0.30 eV of molecular ion binding, i.e., $[NaXe^+] \cong n_e$. We have then systematically varied T_e, n_R, and k_a. We will illustrate the effect of these parameters, and of including $NaXe^+$ dissociative recombination, in the examples shown in Figs. 4 and 5. The effects of variations in the stimulated emission rate caused by external radiation are shown in Fig. 6 for the case of n_R = 3P. The calculated values of extracted power densities and laser amplifier efficiency for the n_R = 6 (Saha) case and for n_R = 3P are shown in Fig. 7. Detailed discussions of these results are presented in the following subsections.

a) Excited state densities

In Figs. 4-6 we show results of our calculations in the form of plots of the log of $[Na(i)/g_i]$ versus excitation energy. We use $2\ell_i + 1$ for the statistical weight, neglecting the alkali spin, since the actual ground state Na density then appears on the abscissa. An excited state distribution at the electron temperature (Saha condition) would appear as a straight line in these figures. In all the cases in Figs. 4 and 5 the electron densities are high enough so that Na radiative rates are much slower than electron collisional rates and the $[Na(i)/g_i]$ for the lower energy states do nearly fit a straight line at the electron temperature. However, above the terminal Na^* state of recombination, n_R, the population distribution frequently falls below such a straight line. In this region of excited state energies, electron collisions are exciting Na^* up a ladder of increasing n and then ionizing the higher n levels. The resulting Na^+ forms $NaXe^+$ and Na_2^+, which then dissociatively recombine to $Na(n_R)$ + Na(3S) to complete the cycle (see Fig. 1). Thus, competition between excitation and ionization by electrons and recombination on Na_2^+ results in population ratios $[Na(n+1)]g_n/[Na(n)]g_{n+1}$ for $n > n_R$ whose average behavior is characterized by an excitation temperature between T_e and T. Using predicted scaling based on the Bates' approximation,[13] we find that at

$n_e^2/[Na][Xe] > 10^{-4}$ (for the $n_R = 6$, $T_e = 0.3$-0.5 eV case) this excitation temperature approaches T_e; at much lower $n_e^2/[Na][Xe]$ it should approach T. In a gas discharge near equilibrium, such as a high pressure arc, with $T = T_e$, inverse ionization of Na^+ and dissociative recombination of Na_2^+ would be balanced by the processes of Na excited-state ionization and $Na^* + Na$ associative ionization. However, in the present discharges in cold gas the Na_2^+ density builds up so that additional dissociative recombination occurs and drives the net ionization below the Saha value appropriate to T_e.

In Fig. 4 we show the effect of varying k_a and n_R at a fixed $T_e = 0.38$ eV. The values $[Na]_0 = 6.3 \times 10^{15}$ cm^{-3} and $[Xe] = 4.5 \times 10^{19}$ cm^{-3} are used for the four lower curves in Fig. 4; these values are representative of the densities used in the experiments of Refs. 1 and 20. In the lowest (+) curve, $n_R = 6$ and $k_a = 1 \times 10^{-9}$ cm^3 s^{-1}; the n_R value is indicated by an arrow. Note that the densities follow a $T_e = 0.38$ eV straight line for $n \leq 6$ and dip slightly below this for $n > n_R$. In the next higher (•) case, and k_a is increased to 2×10^{-9} cm^3 s^{-1}. The dip below a $T_e = 0.38$ eV line for $n > 6$ is more pronounced than in the first case because of the faster rate of Na_2^+ formation and dissociative recombination. The effect of changing n_R can be seen as follows. The dashed line results from distributing the dissociative recombination equally between $n_R = 3D$, $4P$, 4, 5, and 6 states, with $k_a = 1 \times 10^{-9}$ cm^3 s^{-1}. Note that the increased difficulty of laddering upward from these levels has caused a major drop in n_e and the density of high-n states. In the (O) case $k_a = 1 \times 10^{-9}$ cm^3 s^{-1} and $n_R = 4S$ is still more strongly bound, causing n_e and the densities of states with high n to drop still further.

To indicate density dependences, the top (×) curve in Fig. 4 again has $n_R = 6$ and $k_a = 1 \times 10^{-9}$ cm^3 s^{-1}, as for the lowest (+) curve, but both $[Na]_0$ and [Xe] have been increased by about a factor of six. These two $n_R = 6$ cases

dip below the Saha (straight) line by about the same amount, indicating that there the density dependence is relatively minor (at constant $[Na]_0/[Xe]$). This is due to a balance between the effective recombination rate (proportional to [Xe]) and the effective ionization rate (roughly proportional to n_e which varies as $[Na]_0$).

The Na_2^+ dissociative recombination rate coefficient k_{DR} was varied slightly in the different cases in Fig. 4, but the consequences are minor since the $NaXe^+ \rightarrow Na_2^+$ ion exchange is the primary recombination rate limiting step. The value $k_{DR} = 2 \times 10^{-7}\ (0.026/T_e)^{1/2}$ was used for the cross and plus cases in Fig. 4, $k_{DR} = 1 \times 10^{-7}\ (0.026/T_e)^{1/2}$ for the open circle case, $k_{DR} = 5 \times 10^{-8}\ (0.026/T_e)^{1/2}$ for the solid circle case, and $k_{DR} = 2 \times 10^{-8}\ (0.026/T_e)^{1/2}$ to each state from 3D to 6 for the dashed-line case.

In Fig. 5 we show T_e dependence, for $[Na]_0 = 3.5 \times 10^{16}\ cm^{-3}$ and $[Xe] = 2.7 \times 10^{20}\ cm^{-3}$ as would be appropriate for excimer lasers. We have used n_R = 3P examples to illustrate departures from the Boltzmann equilibrium for higher T_e, i.e., for $n_R > 3D$ the densities would satisfy a Boltzmann equilibrium at all n in the $T_e = 0.52$ eV case. In the n_R = 3P, $T_e = 0.52$ eV case (open circles in Fig. 5) the Na^* densities fall about a decade below the Saha limit at high n, while in the $T_e = 0.43$ eV case they drop about 5 decades below this limit. This abrupt change from near Saha equilibrium to severely depleted $[Na^*]$ occurs for any n_R; for higher n_R the critical T_e is lower. The abruptness of this change is due to strong positive feedback: an increase in the laddering-ionization rate coefficient with T_e raises n_e, which further enhances the ionization rate. In the final example in Fig. 4 (▽) we have added rapid $NaXe^+$ dissociative recombination to show the major effect this has. Since in this case the recombination does not proceed via the relatively slow $NaXe^+ + Na \rightarrow Na_2^+ + Xe$ process it very effectively depresses n_e and the $[Na^*]$ at high n values.

The relative Na^* densities for n = 12-15 in our model are normally (for $n_e > 10^{15}$ cm^{-3}) determined by T_e, since the $n \rightleftarrows n + 1$ collisional mixing rates increase rapidly with increasing n, and greatly exceed the dissociative recombination flux for n > 10. Thus all states above n = 12 closely follow a T_e slope. From the Saha condition, which must hold for the very high n, we have from Eq. (1)

$$[Na^*/g^*]_\infty = \left(2\pi mkT_e/h^2\right)^{-3/2} [Na^+]n_e/2g^+ \quad , \qquad (2)$$

where $[Na^*/g^*]_\infty$ is the $n \rightarrow \infty$ limit of $[Na(n)]/g_n$ and $g^+ = 1$ is the Na^+ statistical weight. Thus, the calculated n_e and $[Na^+]$ should yield a $[Na^*/g^*]_\infty$ from Eq. (2) that is consistent with the n = 12-15 values of $[Na(n)]/g_n$. Using Eq. (2) we have calculated the $[Na^*/g^*]_\infty$ points at the Na ionization limit in Figs. 4 and 5, and it can be seen that these fit an extrapolation of the n = 10-15 densities.

One can also use the experimental n_e from Ref. 1 and a calculated $[Na^+]/n_e$ value to obtain an experimental value of $[Na^*/g^*]_\infty$ from Eq. (1). For the $[Na]_0 = 6.3 \times 10^{15}$ cm^{-3} and $[Xe] = 4.5 \times 10^{19}$ cm^{-3} case the ratio $[NaXe^+]/[Na^+]$ is expected to be near the equilibrium value of $K_{eq}^+[Xe] \cong 0.4$ and $[Na_2^+] \ll n_e$, so that $[Na^+] + [NaXe^+] + [Na_2^+] = n_e$ yields $[Na^+] \cong n_e/1.4$. Using this relation in Eq. (2) with the experimental n_e yields an experimental point at the Na ionization limit. (The n_e are calculated in Refs. 1 and 20 from measured current densities and E/N values and calculated electron mobilities.[21]) For the data in Fig. 6 of Ref. 1 $n_e = 2 \times 10^{15}$ cm^{-3} and 3.5×10^{14} cm^{-3} respectively for the 0.38 and 0.33 eV cases. The resulting ionization-limit points, at 5.14 eV, are $\sim 4 \times 10^9$ cm^{-3} for the T_e = 0.38 eV case and $\sim 2 \times 10^8$ cm^{-3} for the 0.33 eV case, i.e., the 0.38 eV point falls slightly below the extrapolation of the 0.38 eV Saha line in the figure of Ref. 1, while the 0.33 eV point falls about a factor of 4 below the 0.33 eV Saha line.

In the Tℓ case we do not have even an estimate of K_{eq}^{+} for $T\ell Xe^{+}$, although the rapid decrease in $[T\ell^{*}/g^{*}]$ above 4.5 eV in Fig. 8 of Ref. 20 suggests that K_{eq}^{+} is much larger than for $NaXe^{+}$ and the effective energies of the $T\ell^{*}(n_R)$ states are near 4.5 eV. Since n_e is an upper limit for $[T\ell^{+}]$, one can still obtain an upper limit to $[T\ell^{*}/g^{*}]_{\infty}$ using $[T\ell^{+}] = n_e$ and the experimental n_e in Eq. (2). This has been done in Fig. 8 of Ref. 20, where it can be seen that it confirms the existence of a major falloff of the high-n densities relative to the Saha condition. These Tℓ data bear considerable resemblance to some of the calculated curves in Figs. 4 and 5.

b) Stimulated emission and efficiency

For metal-excimer laser operation, one would like to obtain a large population in the first excited state, corresponding to a high excitation temperature, i.e., $T_e > 0.5$ eV for the Na case. If the higher levels are also at T_e, however, most of the neutral metal atoms will be ionized. One solution to this problem is to increase $[Na]_0$; then the Saha relation [Eq. (2)] forces the ionization balance toward a smaller fractional ionization. The medium gain in the Saha limit is considered in Sec. IID. Another possible solution occurs if the high-n levels are depressed, relative to Boltzmann equilibrium at T_e, by dissociative recombination, as in some cases in Figs. 4 and 5. In order to explore this latter possibility in detail we have included stimulated emission in the model. We continue to use a K_{eq}^{+} of ~10 times the value for $NaXe^{+}$ in order to represent systems in which dissociative recombination can drive the high Na^{*} and n_e below the Boltzmann equilibrium values. The expected n_R are of course unknown, but states bound by up to 2.5 eV are expected in the Na case and the following results are not very sensitive to the choice of n_R = 3P (bound by 3 eV) and 4S (bound by 2 eV). Thus we use n_R = 3P in the following illustrative example.

In the two-temperature model with weakly bound excimers,[22] the ratio of excimer band stimulated emission cross section $\sigma_s = g_\nu/[Na(3P)]$ to absorption cross section $\sigma_a = k_\nu/[Na(3S)]$ is given by (1/3) exp $[h(\nu_0-\nu)/kT]$, where ν_0 is the atomic transition frequency. The open circle case of Fig. 6 involves high laser powers, where the absorption and stimulated emission rates are almost equal. For this condition [Na(3S)]/[Na(3P)] is driven to the above ratio, which corresponds to an Na(3P) excitation temperature of $T\ \nu_0/(\nu_0-\nu)$. For 700 nm radiation and T = 750 K the quantity $T\ \nu_0/(\nu_0-\nu)$ is ~0.40 eV. We use T_e = 0.52 eV in the examples to be given, so the laser-induced transition between 3S and 3P drives the [Na(3P)]/[Na(3S)] population temperature from 0.52 eV toward 0.4 eV, thereby extracting power from the medium. This transition in the population ratio occurs when the stimulated emission rate equals or exceeds the electron quenching rate for Na(3P) atoms. One can thus estimate the maximum power available for extraction as about equal to that going into 3P quenching by electrons; the following calculations confirm this expected behavior.

We have calculated excited state densities and excimer band stimulated and absorbed power densities as a function of incident flux I for a 700 nm wavelength, T_e = 0.52 eV, and [Xe] = 2.7×10^{20} cm^{-3} using gain and absorption coefficients $g_\nu/[Xe][Na(3P)] = 5 \times 10^{-38}$ cm^5 and $k_\nu/[Xe][Na(3S)] = 7.5 \times 10^{-40}$ cm^5 from Ref. 5 for T = 750 K. For $[Na]_0 = 2.7 \times 10^{17}$ cm^{-3} the resulting Na^* population distributions are given in Fig. 6 while the output powers and efficiencies are given as a function of incident radiation power by the solid curves in Fig. 7. (This incident power would be inter-cavity power in a self-oscillator.) The sharp peaks in the stimulated power and the abrupt increases in efficiency in the n_R = 3P cases in Fig. 7 are due to a sudden drop in n_e by about an order of magnitude, as seen in Fig. 6. This occurs because the [Na(3P)]/[Na(3S)] ratio is lowered by the laser power. Since

ionization occurs by multistep excitation from Na(3P), n_e is therefore forced to decrease, and this also makes the multistep ionization less rapid, which further decreases n_e. At fixed T_e the discharge can thus undergo a type of phase transition, from highly ionized Na and large n_e to slightly ionized Na and low n_e. In the $[Na]_0 = 3.5 \times 10^{16}$ cm^{-3} case, also shown in Fig. 7, this transition to low n_e occurs at a lower incident radiation field. Thus far, our models have examined this effect only at a fixed T_e corresponding approximately to a fixed discharge voltage. If the power supply had an internal impedance comparable with or greater than the discharge impedance the discharge voltage would rise, causing an increase in T_e and tending to maintain n_e near a constant value. The net gain, extracted power, and efficiency should then be larger than indicated in Fig. 7. The maximum net gain coefficient in Fig. 7 is $g_\nu - k_\nu \cong 0.03$ cm^{-1} with $g_\nu \cong 0.05$ cm^{-1} for $[Na]_0 = 2.7 \times 10^{17}$ cm^{-3}. It is important to note that each excimer emission event transfers a fraction $(\nu_0-\nu)/\nu \cong 0.19$ of the photon energy into gas heating, whereas an absorption event causes an equal amount of gas cooling. Therefore the efficiency is not severely limited by the net stimulated emission in the excimer band.

For comparison, we have also indicated in Fig. 7 (short and long-dashed curves) the stimulated power that would be extracted if $n_R = 6$, still with the larger K^+_{eq}. In this case n_e and all $[Na^*]$ are very near the Saha values. These stimulated powers rise smoothly with increasing incident flux, as n_e is nearly constant. At low fluxes net gains are approximately 0.015 cm^{-1} and 0.006 cm^{-1} for $[Na]_0$ values of 3.5×10^{16} and 2.7×10^{17} cm^{-3}. At high incident fluxes the calculated discharge efficiency approaches about 60%, with the energy lost primarily by thermalization of the X and A states of NaXe following stimulated emission and by electron excitation of molecular ions.

The maximum efficiency for extracted power in the n_R = 3P cases of Fig. 7 is also ~60%, with 19% going into gas heating during rethermalization of the NaXe molecules and with the remaining ~20% going primarily into dissociative recombination of electrons and Na_2^+ ions. This large efficiency is the result of the large rates of Na(3P) deexcitation collisions and of the consequent large rate of saturated stimulated emission compared to the effective rate of ionization for Na(3P) atoms. The maximum extracted power at ~350 MW/cm^2 incident laser flux is ~10 MW/cm^3 or 10^3 J/ℓ in an 0.1 μsec pulse. (The pulse length is limited to ~0.1 μsec by gas heating.) We must reemphasize that this model applies to a hypothetical excimer with $K_{eq}^+ > 10^{-19}$ cm^2 and in which the equivalent of $e + Na_2^+ \rightarrow Na(3P) + Na(3S)$ occurs. Furthermore, as discussed in Sec. IIC, the model does not contain an unknown process that is responsible for approximately 75% of the discharge energy reported in the measurements of Refs. 1 and 20.

C. DISCHARGE ENERGY BALANCE AND V-I CURVES

Once the kinetics have been established (see Sec. IIB), one expects to be able to write down the energy balance for the metal-rare gas discharge. In principle the energy balance can be used to derive volt-ampere curves for the discharge. However, we will show that the energy loss processes considered in our model do not add up to the experimental energy input so that there must be energy loss mechanisms that we have not considered. Only the dominant energy loss processes are discussed here.

The electron energy balance equation relevant to the present problem is

$$JE = \sum h\nu R_\nu + \nu_u k(T_e - T)n_e + (\varepsilon_R + 3kT_e/2)\alpha_{DR} n_e [Na_2^+]$$

$$+ (\varepsilon_R' + 3kT_e/2)\alpha'_{DR} n_e [NaXe^+] + \sum \varepsilon_{ij} k_{ij} n_e [NaXe^+] \quad . \qquad (3)$$

Here the power input to the electrons is JE, where J is the current density and E the electric field. The first term on the right-hand side is the net radiative energy loss, the second term is due to elastic recoil of Xe atoms, the third and fourth terms are due to dissociative recombination of Na_2^+ and $NaXe^+$, and the last term represents vibrational and rotational excitation of $NaXe^+$. R_ν is the rate (cm^{-3} s^{-1}) of escape of photons of energy $h\nu$ and ν_u is the frequency of energy exchange collisions of electrons of temperature T_e with the neutral atoms of temperature T. Also, ε_R and ε_R' are the average ionization energies of excited atoms produced by dissociative recombination of electrons and Na_2^+ and $NaXe^+$ ions respectively with rate coefficients α_{DR} and α_{DR}' respectively. ε_{ij} and k_{ij} are the energy transferred and rate coefficient associated with electron impact excitation of $NaXe^+$ from vibrational-rotational level i to level j. Note that the first, third and fourth terms on the right-hand side of Eq. (3) replace the large number of terms representing the electron energy loss and gain in excitation and deexcitation collisions with metal atoms.

The radiative loss term in Eq. (3) includes spontaneous emission and stimulated emission and absorption via the excimer band. Since we have assumed that the upper and lower molecular states of the excimer transition are maintained in thermal equilibrium with the respective atomic states, the energy supplied by the electrons per excimer photon emitted is equal to the excitation energy of the atomic resonance state. Experiments[1,20] and our calculations show that the contribution of spontaneous radiation for wavelengths between 200 and 800 nm is only a few percent of the discharge power, and we believe that radiative losses are still negligible when shorter and longer wavelengths are included. As noted in Sec. IIB, for Na the net gas heating is 19% of the optical energy extracted at 700 nm.

The rate coefficient for energy exchange collisions in Eq. (3) is roughly equal to $(2m/M)\langle\sigma_m v\rangle[Xe]$ for electron temperatures of interest in this paper, i.e., the electrons lose energy by elastic recoil of the Xe atoms. Here m and M are the electron and Xe atom masses and $\langle\sigma_m v\rangle$ [Xe] is the average frequency of momentum transfer collisions of electrons with Xe atoms. Using the cross-section data from Ref. 21, we obtain a normalized energy exchange collision frequency $\nu_u/[Xe] = 1.5 \times 10^{-12} (T_e)^{1.6}$ cm^3/sec^{-1} for T_e between 0.3 and 1 eV. We then find that for the experimental $n_e = 2 \times 10^{15}$ cm^{-3} of the 0.38 eV case in Ref. 1, the energy lost by elastic recoil is about 10% of the experimental power input of about 16 kW/cm^3.

Since the Na_2^+ dissociative recombination rate is limited by the ion exchange rate k_a, the contribution of dissociative recombination to the energy balance can be estimated as $k_a[Na][NaXe^+]\Delta E$, where the energy loss per recombination $\Delta E = 3kT_e/2 + \epsilon_R$, i.e.,

$$\alpha_{DR} n_e [Na_2^+] = k_a [Na(3S)][NaXe^+] \quad . \tag{4}$$

Using a mean value of ~1 eV for ϵ_R, $[NaXe^+] = n_e K_{eq}^+ [Xe]/(1 + K_{eq}^+ [Xe])$ and $k_a = 10^{-9}$ cm^3 s^{-1} yields recombination energy losses which are typically about 4% of the experimental energy input for the 0.38 eV data of Ref. 1. (In the limit of $K_{eq}^+ [Xe] \gg 1$, where K_{eq}^+ refers to $T\ell Xe^+$, the recombination energy loss is about 20% of the total energy input for the Tℓ-Xe discharge data of Ref. 20). If $NaXe^+$ dissociative recombination to a high n_R (e.g., 8) is added, the energy loss via dissociative recombination is increased by a large factor without significantly changing n_e or the measured Na^* values. Thus adding $NaXe^+$ recombination at high n, typically with a rate coefficient α_{DR} of about half the Na_2^+ value, is one way to explain the measured powers. However, as indicated in Sec. IIA theoretical arguments predict α_{DR} of $NaXe^+$ to be much smaller and this contribution to the energy balance to be negligible.

(This also applies to Tℓ-Xe, and to any metal whose ionization energy is less than the Xe excitation potential.)

Based on the theory of Ref. 23, rotational and vibrational excitation of the dominant molecular ion $NaXe^+$ appear to be a small (~2%) but not negligible energy drain. Other energy loss processes considered but rejected as too small to be of importance in Eq. (3) were a) collisions between two excited atoms; b) inverse ionization and collisional deexcitation down the NaXe molecular excited state ladder to the $NaXe(A^2\Sigma)$ state followed by dissociation and then by electron induced excitation and ionization up the atomic excited state ladder; c) quenching of Na^* states due to Xe collisions with a rate coefficient of about 10^{-10} cm^3/sec^{-1}; d) dissociation of molecules by electron impact; and e) free-free radiation, which has been calculated[24] and also could be detected at wavelengths below 1 μm if it were large enough to yield a significant energy loss. We therefore calculate a total energy loss rate for the T_e = 0.38 eV case of Ref. 1 of less than 25% of the measured power input. A similar discrepancy is found for the T_e = 0.33 eV case.

An alternative means of examining the energy balance is to derive an expression for the electric field versus current density, or more commonly, the volt-ampere curve for the discharge. We first note that the current density is given by the relation (N=[Xe])

$$J = en_e\mu_e N(E/N) \quad , \tag{5}$$

where $\mu_e N$ is the electron mobility normalized to unit density. When Eqs. (4) and (5) are substituted in Eq. (3), with radiation neglected, one obtains the equation

$$e\mu_e N(E/N)^2 = (\epsilon_R+3kT_e/2)k_a[Na(3S)]/N + (\nu_u/N)k(T_e-T)$$

$$+ \{(\epsilon_R'+3kT_e/2)\alpha_{DR}' + \Sigma\epsilon_{ij}k_{ij}\}(J/N)\{e\mu_e N(E/N)\}^{-1} \quad . \tag{6}$$

From Eq. (6) one sees that when the energy loss is due only to Na_2^+ dissociative recombination and Xe elastic recoil [first two terms on the right side of Eq. (6)], E/N depends on the discharge current density only through the rather slow changes in electron temperature with J. Experimental measurements[1,20] show that E/N increases much more rapidly with J than predicted from the temperature increase of these terms. When the last term in Eq. (6) dominates, the E/N varies approximately with $(J/N)^{1/3}$. Approximate agreement in magnitude and J/N variation with the initial voltage-current data, before measurements of cathode fall, led us to the no longer tenable hypothesis[22] that dissociative recombination of electrons with $NaXe^+$ was the dominant energy loss mechanism in the experimental discharges. However, this now appears to be very unlikely as are other possible causes we have investigated, such as rotational and vibrational excitation of $NaXe^+$.

D. GAIN COEFFICIENT IN THE SAHA-BOLTZMANN LIMIT

The primary objective of this section is to explore the consequences of assuming that $[Na^+]$, n_e, [Na], and all $[Na^*]$ are in Saha-Boltzmann equilibrium ratios at temperature T_e. As in the previous sections we assume that atomic translation and molecular vibration temperatures are at the gas temperature T, so that gain in the excimer band results at a sufficient excited state density, as in the two-temperature model of Ref. 22. As suggested in Sec. IIB, a rapid improvement in laser gain with increasing $[Na]_0$ is predicted. In the Tℓ-Xe case, the data indicate that less ionization actually occurs, perhaps due to a larger binding of $TlXe^+$ compared to $NaXe^+$. A modification to this simple two-temperature model for this case will be discussed at the end of this section.

As was found in the detailed model, we assume that $Na^+ + 2Xe \rightleftarrows NaXe^+ + Xe$ is in equilibrium at the gas temperature, i.e.,

$$\frac{[NaXe^+]}{[Na^+]} = [Xe]K_{eq}^+(T) \quad , \tag{7}$$

where we use $K_{eq}^+(T) = 6 \times 10^{-23}\ (T/670\ K)^{1/2}\ \exp(0.3\ eV/kT)\ cm^{-3}$. From the calculations of Sec. IIB we find that $[Na_2^+]/[Na^+] \ll 1$, as expected due

to slow formation and rapid depletion of Na_2^+ at $n_e > 10^{15}$ cm^{-3}. Thus, using Eq. (7),

$$n_e = [Na^+] + [NaXe^+] + [Na_2^+] \cong [Na^+]\{1+[Xe]K_{eq}^+(T)\} \quad . \qquad (8)$$

Combining Eqs. (1) and (8), we obtain

$$n_e^2 \cong \kappa\{1+[Xe]K_{eq}^+(T)\}[Na(3S)]\left(2\pi mkT_e/h^2\right)^{3/2} \exp(-E_I/kT_e) \quad , \qquad (9)$$

If we take into account neutral depletion, i.e., $[Na(3S)] \approx [Na]_0 - n_e - [Na_2^+] \approx [Na]_0 - n_e$ then the electron temperature is given approximately by the solution of the relation

$$e^{-E_I/kT_e} = \frac{n_e^2/([Na]_0 - n_e)}{(2\pi kT_e/h^2)^{3/2}\{1+[Xe]K_{eq}^+(T)\}} \quad . \qquad (10)$$

Assuming equilibrium between the Na(3P) and Na(3S) densities at T_e, we see that the [Na(3P)] density can then be expressed as

$$\frac{[Na(3P)]}{3([Na]_0 - n_e)} = \exp[-E(3P)/kT_e] = [\exp(-E_I/kT_e)]^{2.1\ eV/5.14\ eV} \quad . \qquad (11)$$

When Eq. (11) is substituted into the expression for the net gain, i.e., $G = \sigma_s[Na(3P)] - \sigma_a[Na(3S)]$ one obtains the relation

$$\frac{G}{\sigma_s} = [Na]_0(1-\chi)\left[\frac{B\chi^{2\alpha}}{(1-\chi)^{\alpha}} - \frac{\sigma_a}{\sigma_s}\right] \quad , \qquad (12)$$

where $\chi = n_e/[Na]_0$, $B = 3[Na]_0^{\alpha}[(2\pi mkT_e/h^2)^{3/2} \times (1+[Xe]K_{eq}^+)]^{-\alpha}$, and $\alpha = 2.1/5.14 = 0.41$. Since B varies slowly with T_e, most of the variation in gain with electron temperature has been absorbed into the variation with electron density. We therefore maximize the gain in Eq. (12) with respect to electron density at constant B to obtain the maximum gain values shown in Fig. 8. Note that n_e is a controllable experimental parameter determined primarily

by the discharge current density. At high radiative fluxes the Na(3P) and Na(3S) densities are no longer in equilibrium and one must use a more detailed model, such as that of Sec. IIB.

Figure 8 indicates that very large gain coefficients might be achieved at higher Na densities than those investigated in Ref. 1 (10^{15}-10^{16} cm^{-3}). However, two major problems with the higher density regime are the rapid gas heating and the low discharge impedance. Using the relations given in Sec. IIC for the energy dissipation and the conditions given in Fig. 8 for an optical gain of 0.02 cm^{-1}, we calculate rates of rise of gas temperature of about 2000 K/μsec. The corresponding discharge resistivity is 0.07 ohm-cm. Because of the unexplained excess energy losses in the experimental discharges[3] discussed in Sec. IIC the actual rate of rise of gas temperature and the discharge impedance could be significantly larger than these values. Thus, while the gain and excitation temperature are very favorable at $n_e \approx [Na] \approx 10^{17}$ cm^{-3} the power dissipation would limit the discharge pulse length to about 100 nsec. Of course, this is just a statement of a universal problem: Any device with an efficiency ε for laser power extraction and an allowable gas heating of ΔT will be limited to pulse energy densities of $c_p N \Delta T$ and extracted energy densities of $\varepsilon c_p N \Delta T$, where c_p is the specific heat and N the density of the gas.

The Tℓ doped-Xe experiment in Ref. 20 indicated that $[Tℓ^+]$ and the higher $[Tℓ^*]$ are below the Saha or equilibrium values at T_e (see Ref. 20, Fig. 8). According to our model this indicates that $K_{eq}^+[Xe] \gg 1$ for $TℓXe^+$. This reduction of $[Tℓ^+]$ below the Saha value by a factor $F < 1$ can be accounted for in Eqs. (1), (7)-(11) by multiplying the right side of Eq. (1) by F. The quantity $(1 + K_{eq}^+[Xe])$ in Eqs. (9), (10), and (12) is then multiplied by F. In Sec. IIB we tested for the effect of such an increase in K_{eq}^+ by

increasing that for $NaXe^+$ by a factor of 10-20. Some reduction in $F(1 + K_{eq}^+ [Xe])$ did occur, but the consequence in Eq. (12) was less than 50% reduction in the gain shown in Fig. 8. This is in part because increasing K_{eq}^+ increased the effective dissociative recombination rate and thereby decreased F. Thus the optimum gain appears to be almost independent of the size of K_{eq}^+, although the energy dissipated in the ionization-recombination loop is directly proportional to K_{eq}^+.

E. CONCLUSIONS

We have modeled a very high-power density electric discharge in a nonequilibrated vapor consisting of low ionization-potentials atoms (Na or Tℓ) doped into a high ionization-potential atomic gas (Xe). It was necessary to include a large number of excited-state species, plus several ion and molecular species. At the lower T_e considered the principal mechanism controlling the discharge impedance is multistep ionization from a state of principal quantum number n_R, followed by molecular ion formation and dissociative recombination back to n_R. Comparison to Tℓ excited-state densities in a Tℓ-doped Xe discharge indicates that n_R values as low as 3 occur for this case. In the Na-Xe discharge case it is not possible to infer n_R because the small K_{eq}^+ causes relatively small departures from Saha densities at T_e. In the Na case the measured discharge power typically exceeds that in the model by a factor of four. Electron-Xe elastic recoil, Na_2^+ dissociative recombination, radiation, quenching of excited Na and NaXe states, and rotational and vibrational excitation of $NaXe^+$ were considered. As yet we have no explanation for this extra power dissipation.

At the $T_e > 0.5$ eV appropriate for NaXe excimer laser operation, the densities of n_e and all Na states are very nearly in Saha equilibrium at T_e, regardless of n_R. Reasonable gain coefficients and efficiencies can be obtained at high $[Na]_0$ under these circumstances, e.g., for $[Na]_0 = 2.7 \times 10^{17}$ cm^{-3} and

$[Xe] = 2.7 \times 10^{20}$ cm^{-3} a maximum gain of 0.03 cm^{-1} and delivered power of 10 MW/cm^3 at an incident radiative flux of 350 MW/cm^2 and an electron density of 10^{17} cm^{-3}. A 10 cm length of such a medium could readily yield a self-excited oscillator, although the power-buildup e-folding time of ∿1 nsec in this low-gain medium must be considered. This conclusion does not depend on an understanding of all the energy-loss mechanisms in the discharge, but the efficiency does. The calculated maximum efficiencies of ∿60% are probably at least a factor of 3 too high, but as we have not identified the dominant energy-loss mechanism or its dependence on n_e and T_e, we cannot reliably estimate the efficiency. The scaling of this gain and power output with $[Na]_0$ and other parameters allows predictions of operating conditions for maximum gain to be made rather simply.

By considering the case of a large K_{eq}^+ value and dissociative recombination of Na_2^+ to produce Na(3P) atoms, we have identified an interesting sort of phase transition in which n_e decreases and [Na] increases by about an order of magnitude at a critical laser power. In addition to raising the discharge impedance, this lower n_e condition would probably yield higher efficiency in a real case since experimental data indicate that the unknown energy-loss mechanism scales as a fairly high power of n_e. These results point to the desirability of finding a metal species M with relatively strong MXe^+ binding for which the dimer ion dissociatively recombines into a strongly bound excited atom and a ground state atom.

III. ELECTRON EXCITATION RATES IN METAL VAPORS

Drs. E. R. Mosburg, Jr. and A. V. Phelps

This new experiment is intended to yield effective rate coefficients for electron collisions with highly excited atoms so as to test models of the high

power density discharges in metal vapor-rare gas for laser applications. We propose to use a tunable dye laser to modulate the density of selected highly excited levels of mercury atoms in a discharge so as to obtain effective electron collision and ionization rate coefficients for these excited states. As indicated in the Report Summary, work on this portion of this contract during the current period was limited to the acquisition of essential equipment.

IV. ELECTRON EXCITATION OF METASTABLE ATOMS AND MOLECULES

Drs. K. Tachibana and A. V. Phelps

During this report period we have designed and constructed an apparatus for the measurement of electron excitation rate coefficients for the $^3P_2$ and $^3P_1$ metastable and resonance states of Ne. A schematic of the experimental apparatus is shown in Fig. 9. The electron drift tube is the same as that used in the measurement of excitation rate coefficients for the $b^1\Sigma$ metastable state of O_2 and the $A^3\Sigma$ and $C^3\Pi$ states of N_2, and is described in detail in Ref. 25. Photoelectrons released from the semitransparent cathode are periodically heated and caused to flow across the drift region by a square wave voltage applied to the anode. The electrons excite the ambient Ne atoms to the metastable and resonance states. These atoms are destroyed by collisions and lost to the electrodes by diffusion of the metastables and by radiation from the resonance atoms.

The time variation of the density of neon metastable and resonance atoms is determined from measurements of the absorption of narrow band radiation (200 MHz) emitted by a single mode dye laser. The dye laser is stabilized to the peak of the neon absorption line using the optogalvanic effect from a commercial Ne hollow cathode discharge lamp.[26] As shown in Fig. 9, the optical system includes a multi-pass (normally 32 passes) cell which gives an active

absorption path of nearly 2 m. Figure 10 shows one of the better absorption transients obtained thus far. In this case the quasi-steady-state metastable density corresponds to about 10^8 metastables/cm^3 and the rms noise signal corresponds to about 10^6 metastables/cm^3.

A second example of the operation of this system is shown in Fig. 11, where the relative fluorescent intensity is plotted as a function of the laser frequency as the laser is tuned through the absorption line profile. The solid dashed curve shows the profile calculated assuming the expected Doppler broadening at room temperature and taking into account the known isotope components. This data illustrates the spectacular improvement in the accuracy of absorption measurements expected with this new technique. Instead of an unknown emission profile from the conventional neon capillary discharge source and a poorly known overlap with the absorption profile, we can now use the narrow and tunable laser source to measure the fluorescence profile and so obtain the absorption profile.

During the next report period we will use this technique to measure metastable and resonance atom absorption transients over a range of Ne densities and E/N values so as to obtain the data necessary for the determination of the electron excitation rate coefficients for these excited states of Ne.

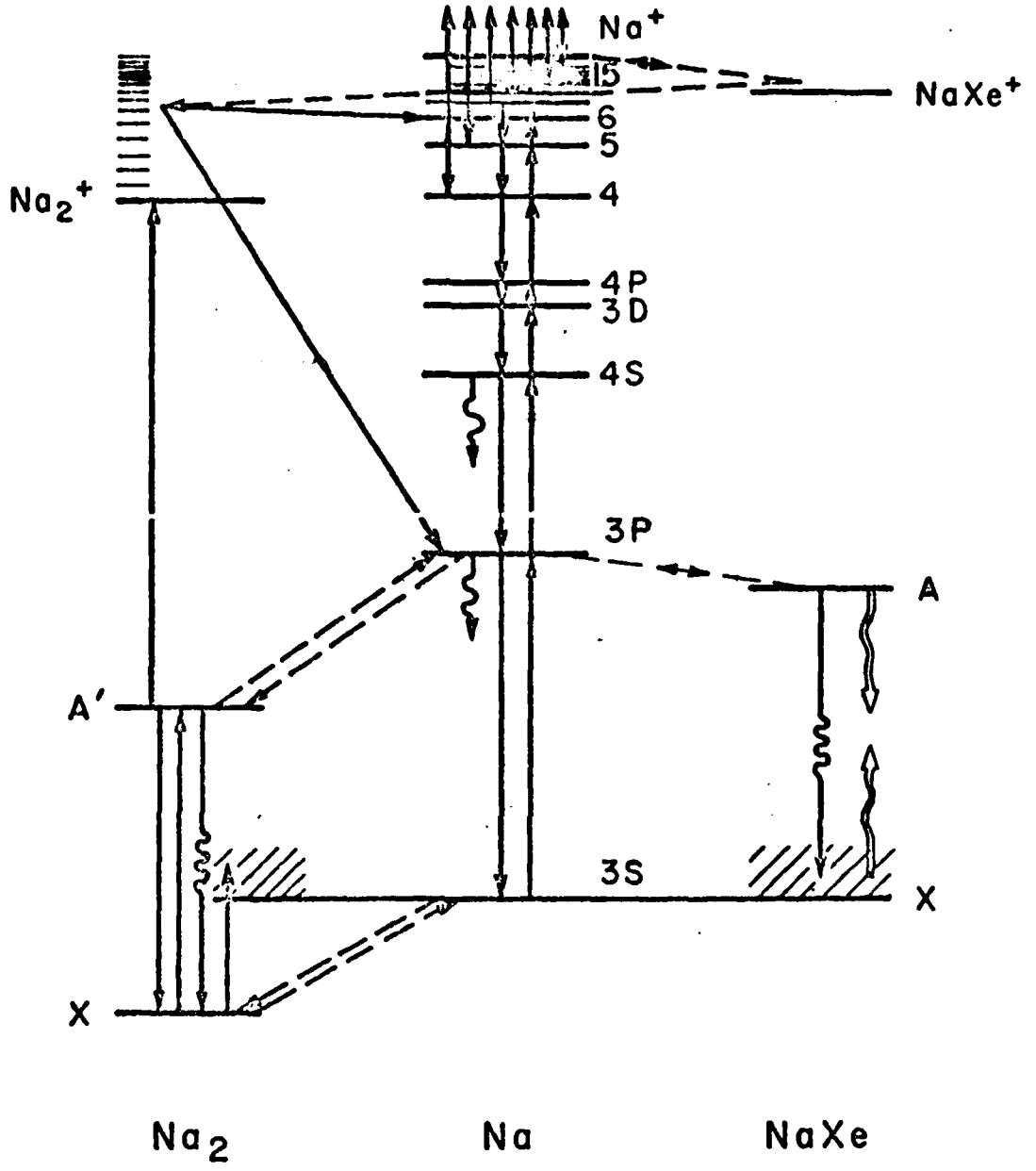

Figure 1 - Energy levels and radiative and collisional processes used in the model. Dashed lines are due to gas collision processes, solid lines to electron collisions, single wavy lines to spontaneous emission, and double wavy lines to absorption and stimulated emission. Ionization from and inverse ionization to all Na levels are included in the model, although only those to higher levels are indicated here. Some vibrational levels of Na_2^+ are indicated, although Na_2^+ is treated as a single state in the calculations. This figure shows the alternate paths for electron-Na_2^+ dissociative recombination leading to Na atoms in the 3P or n = 6 levels.

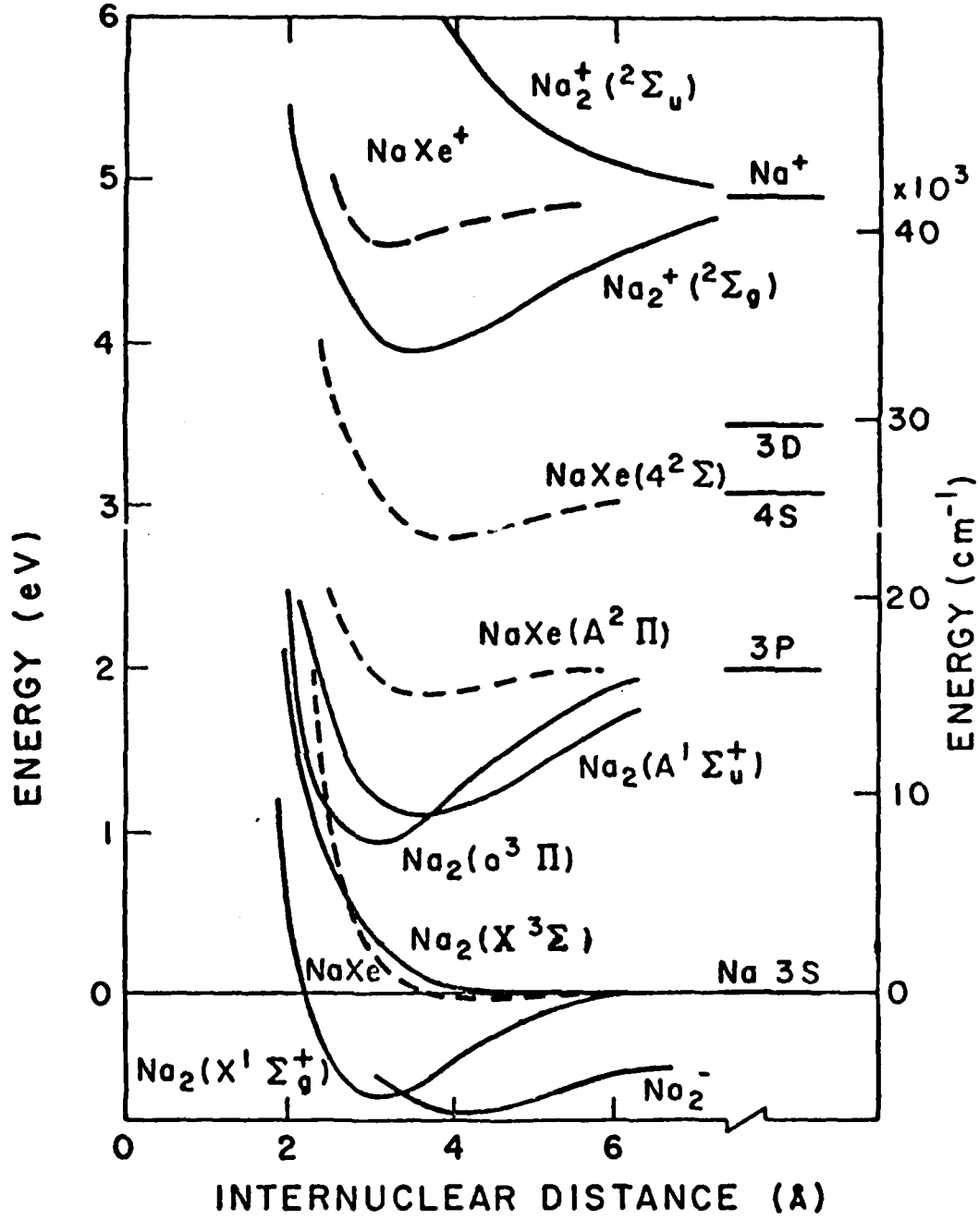

Figure 2 - Electronic energies of various NaXe, Na_2, and Na states. The Na_2, Na_2^+, and Na_2^- potentials are from Ref. 9, $NaXe^+$ from Ref. 7, NaXe and $NaXe(A^2\Pi)$ from Ref. 5, and $NaXe(4\Sigma)$ from Ref. 6.

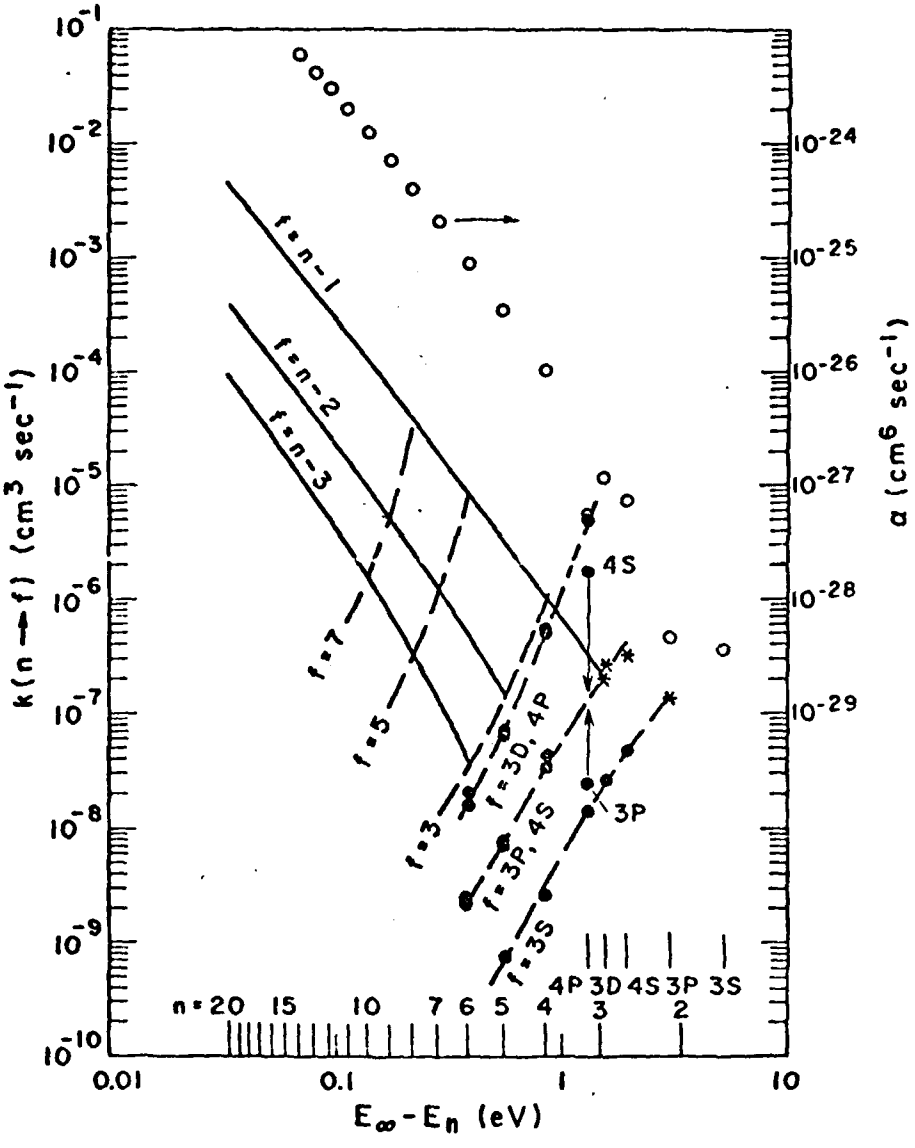

Figure 3 - Deexcitation and inverse ionization rate coefficients used for various states of Na for T_e = 0.38 eV. Excited states above Na(4P) are replaced by hydrogenic equivalents.

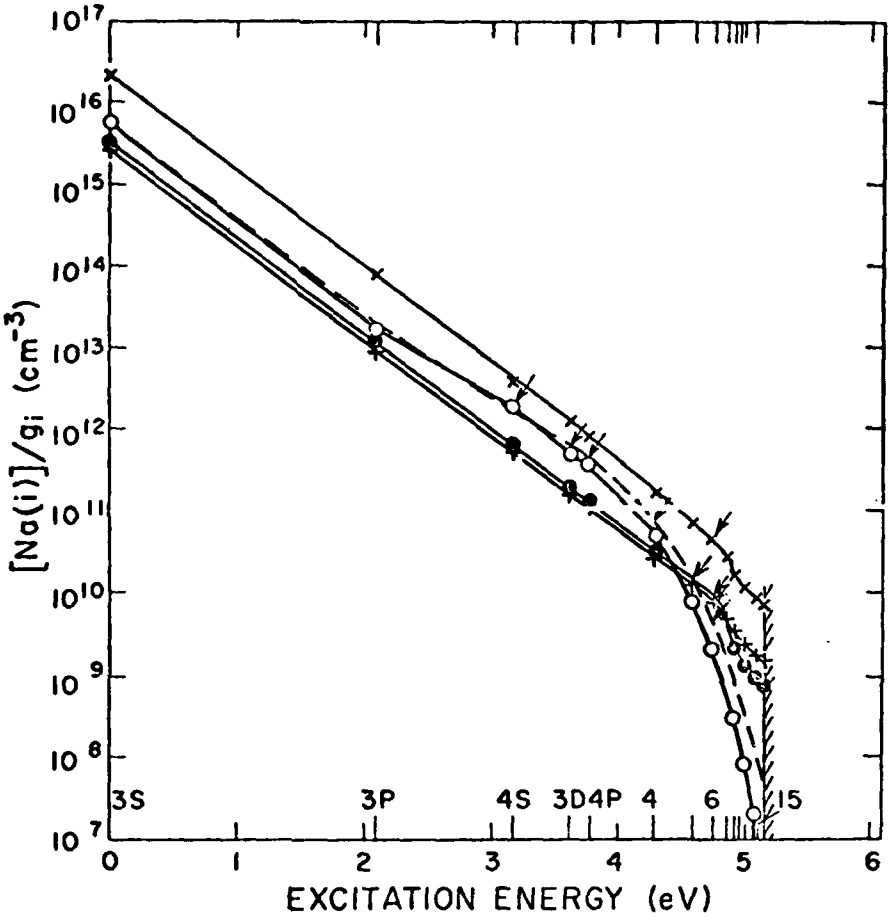

Figure 4 - Calculated Na excited-state densities [Na(i)] divided by $g_i = 2\ell_i + 1$ versus excitation energy. The conditions are $[Na]_0 = 3.5 \times 10^{16}$ cm^{-3} and [Xe] = 2.7×10^{20} cm^{-3} for the top curve, and $[Na]_0 = 6.3 \times 10^{15}$ cm^{-3} and [Xe] = 4.5×10^{19} cm^{-3} for the other cases, with T_e = 0.38 eV in all cases. The states n_R produced by Na_2^+ dissociative recombination are indicated by arrows. For the top and bottom (x and +) curves n_R = 6, and $k_a = 10^{-9}$ cm^3 s^{-1}, resulting in $n_e = 1.4 \times 10^{16}$ and 3.5×10^{15} cm^{-3} respectively. The other (•) n_R = 6 case uses $k_a = 2 \times 10^{-9}$ cm^3 s^{-1}, with the larger k_a causing a decrease in ionization ($n_e = 2.6 \times 10^{15}$ cm^{-3}) relative to the (+) case. In the (0) case n_R = 4S and $k_a = 10^{-9}$ cm^3 s^{-1}, resulting $n_e = 1.1 \times 10^{14}$ cm^{-3}. The dashed line case uses the same k_a combined with Na_2^+ dissociative recombination distributed equally to the 5 states between 3D and 6, resulting in $n_e = 7.4 \times 10^{14}$ cm^{-3}.

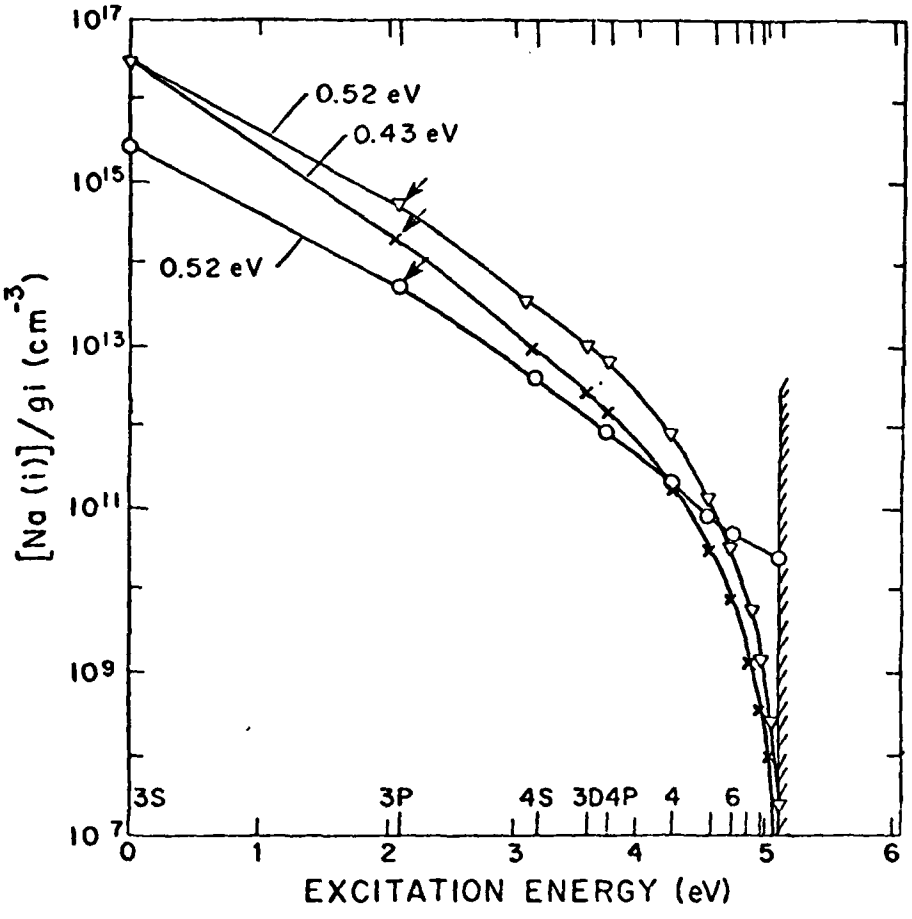

Figure 5 - $[Na(i)]/g_i$ for $[Na]_0 = 3.5 \times 10^{16}$ cm^{-3}, $[Xe] = 2.7 \times 10^{20}$ cm^{-3}, and as a function of the indicated electron temperatures. Na_2^+ dissociative recombination to $n_R = 3P$, as indicated by the arrows, is included with $k_{DR} = 2 \times 10^{-7}\ (0.026/T_e)^{1/2}$ and $k_a \gtrsim 10^{-9}$ cm^3 s^{-1}. $NaXe^+$ dissociative recombination to $n_R = 3P$, with the same k_{DR}, is also included in the upper (∇) 0.52 eV case. The resulting n_e are, from top to bottom, 1.1×10^{15}, 3.5×10^{14}, and 3.2×10^{16} cm^{-3}. The points at the ionization limit represent the electron and ion density through Eq. (2).

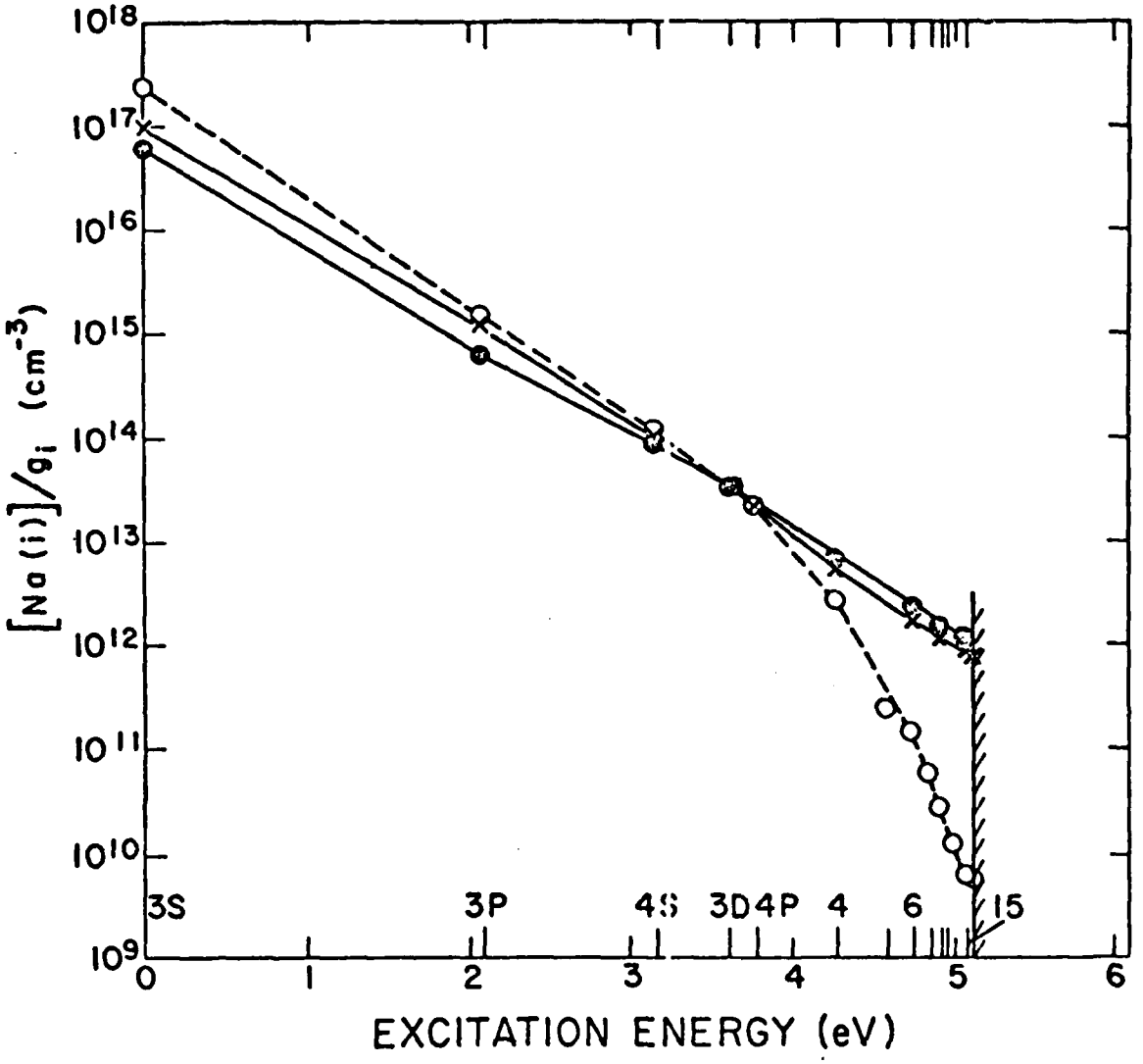

Figure 6 - Same quantities as in Fig. 4 as a function of 700 nm radiation intensity I, with $[Na]_0 = 2.7 \times 10^{17}$ cm^{-3}, $[Xe] = 2.7 \times 10^{20}$ cm^{-3}, $T_e = 0.52$ eV, and $n_R = 3P$. The closed circles are for I = 0, the × for I = 320 MW/cm^2 and the open circles for I = 560 MW/cm^2; the corresponding values of n_e are 2.0×10^{17}, 1.65×10^{17}, and 1.4×10^{16} cm^3, respectively.

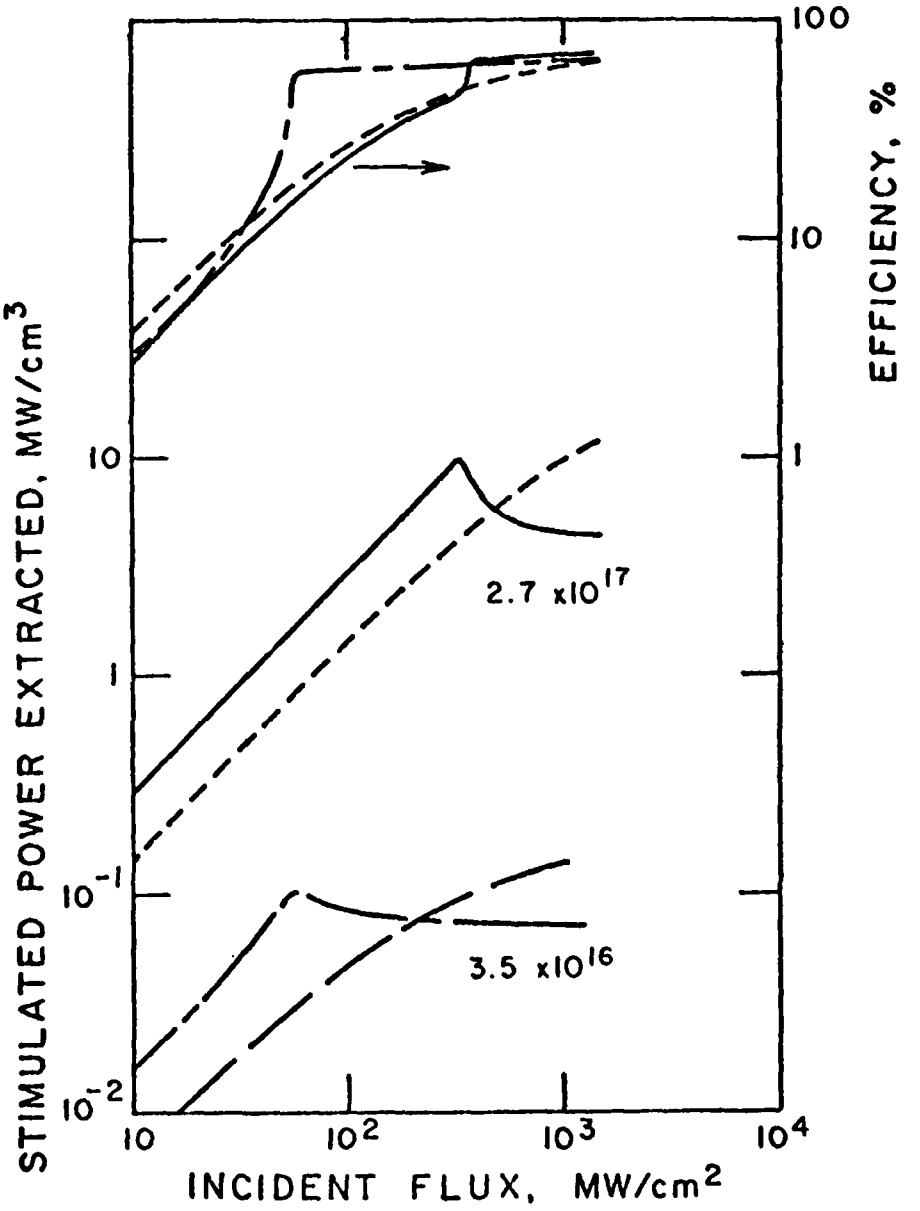

Figure 7 - Stimulated radiative power extracted from the discharge (lower four curves) and laser amplifier efficiency (upper three curves) as a function of incident optical power at 700 nm. The solid curves are for the conditions of Fig. 6. The chain (——— ·) curves are for $[Na]_0 = 3.5 \times 10^{16}$ cm^{-3} and $n_R = 3P$. The long and short dashed curves are for $n_R = 6$ and for $[Na]_0 = 3.5 \times 10^{16}$ and 2.7×10^{17} cm^{-3}, respectively, conditions which result in near Saha values for n_e and all [Na*].

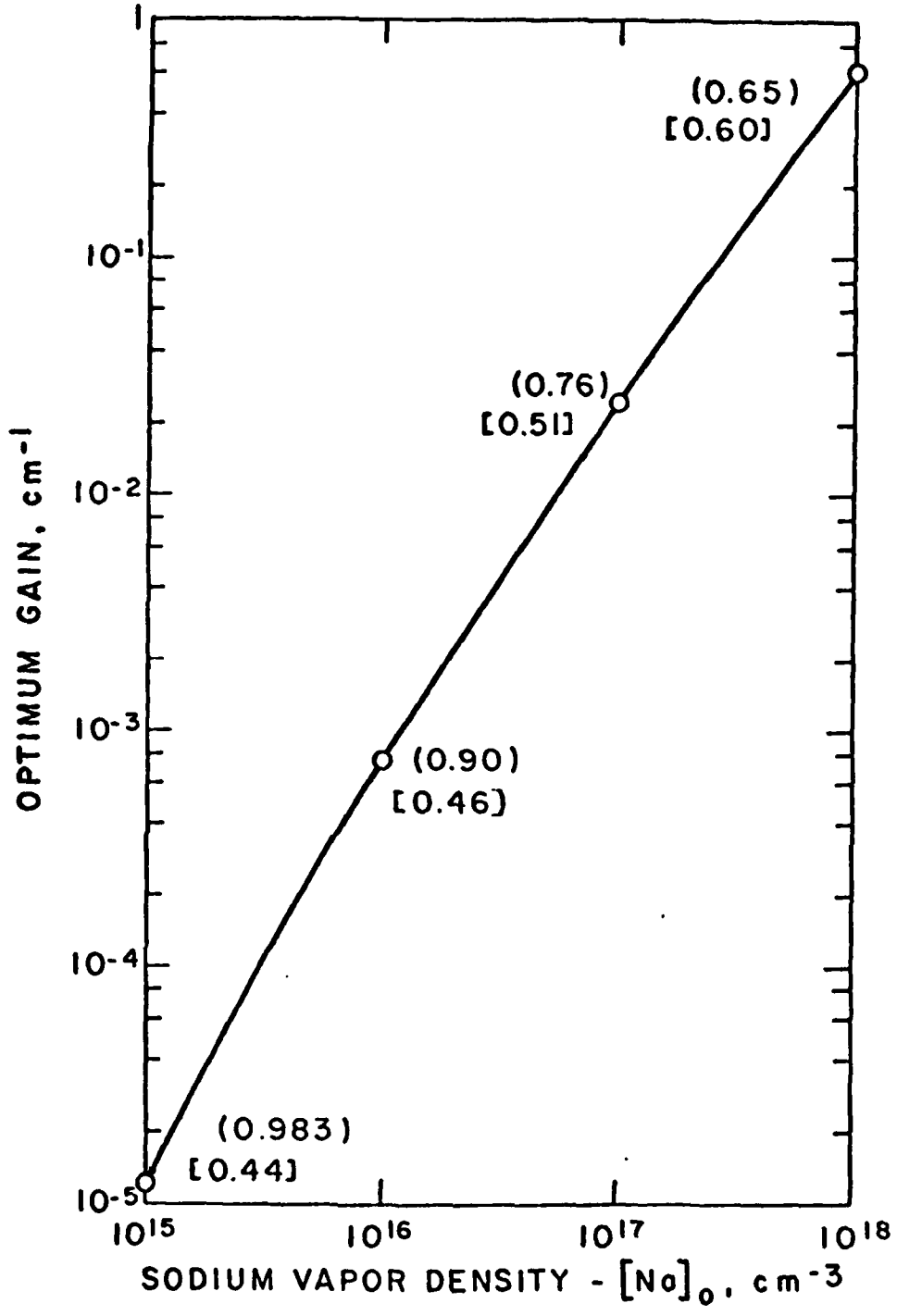

Figure 8 - Maximum net gain versus initial sodium density $[Na]_0$. The numbers in square brackets are the electron temperatures in eV and the numbers in parentheses are the ratios of n_e to $[Na]_0$. F is the ratio of $([Na^*]/g^*)_\infty$ to the Saha equilibrium value.

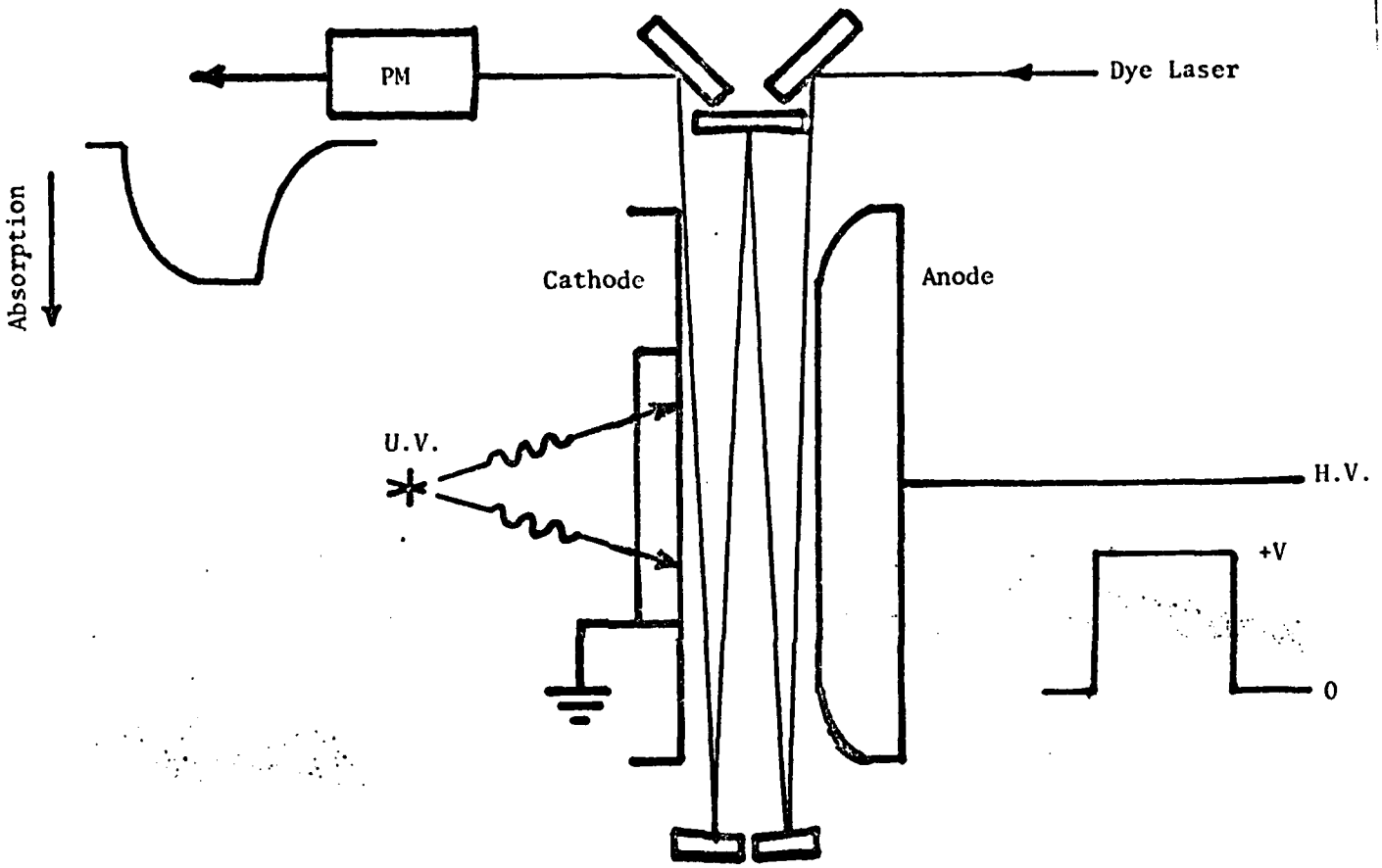

Figure 9 - Schematic of drift tube and absorption optics for measurement of Ne metastable and resonance atom excitation rate coefficients.

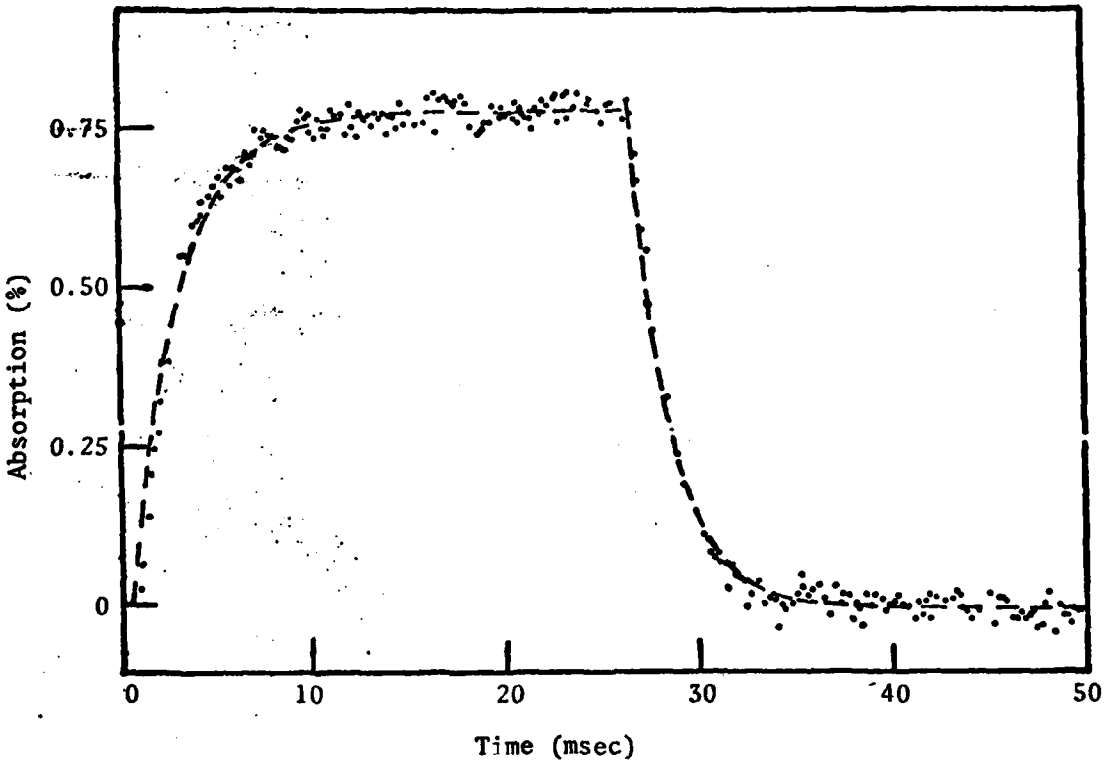

Figure 10 - Example of absorption signal for Ne($^3P_2$) metastable. λ = 588 nm, [Ne] = 6.4×10^{16} cm^{-3}, E/N = 3.7×10^{-16} V-cm^2, Iav = 0.42 μA.

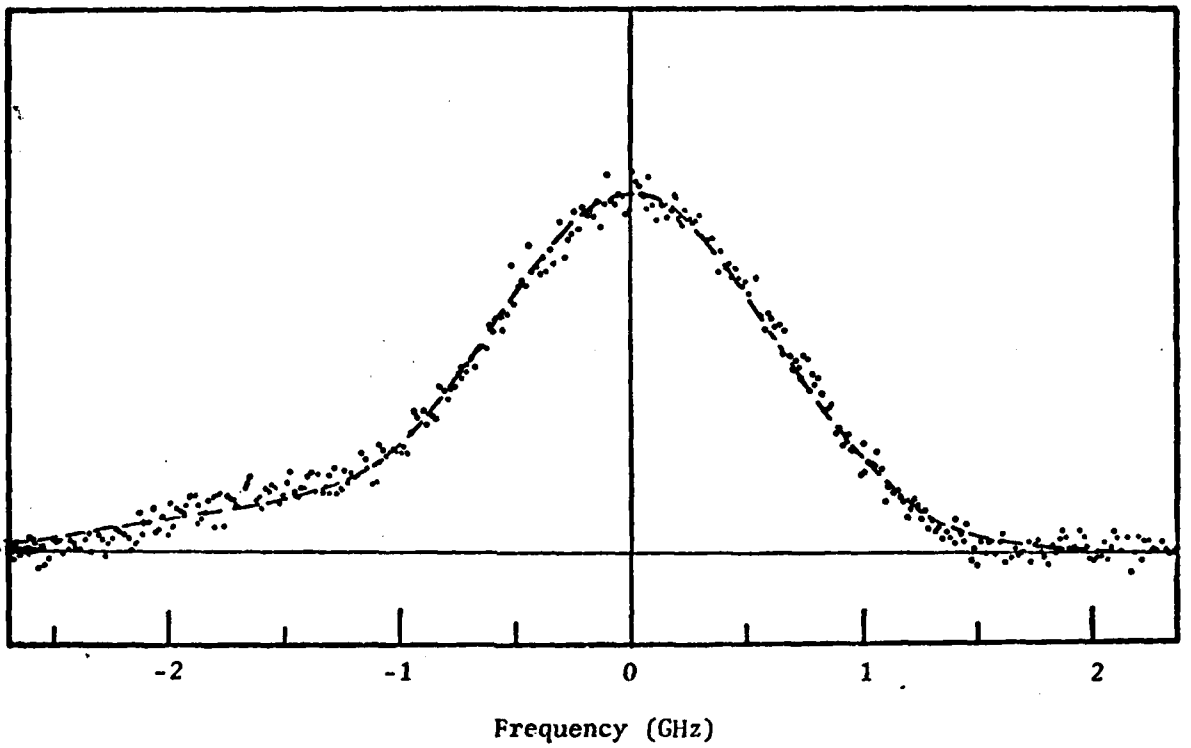

Figure 11 - Fluorescence profile for λ = 588 nm line of Ne as obtained with tunable dye laser. The dashed curve is the normalized theoretical Doppler profile including the isotopic components.

REFERENCES

1. H. Rothwell, D. Leep and A. Gallagher, J. Appl. Phys. 49, 4396 (1978).
2. L. A. Schlie, J. Appl. Phys. 47, 1397 (1976).
3. L. C. Johnson, Astrophys. J. 174, 227 (1972).
4. D. L. Moores, D. W. Norcross and V. B. Sheorey, J. Phys. B 7, 371 (1974). See also D. F. Korf, S. Chung and C. C. Lin, Phys. Rev. A 7, 545 (1973).
5. G. York, R. Scheps and A. Gallagher, J. Chem. Phys. 63, 1052 (1975). The conditions in Fig. 11 are $[Xe] = 2 \times 10^{20}$ cm^{-3}, $[Na(3S)] = 10^{17}$ cm^{-3}, $[Na(3P)] = 5 \times 10^{15}$ cm^{-3}, T = 810 K.
6. A. C. Tam, C. Moe, B. R. Bulos, and W. Happer, Opt. Commum. 16, 376 (1976); A. C. Tam, T. Yabuzaki, S. M. Curry, and W. Happer, Phys. Rev. A 18, 196 (1978).
7. The $NaXe^+$ potential is estimated from the following references: T. R. Powers and R. J. Cross, Jr., J. Chem. Phys. 58, 626 (1973); F. E. Budenholzer, E. A. Gisason, and A. D. Jorgensen, J. Chem. Phys. 66, 4832 (1977); F. A. Gianturco, J. Chem. Phys. 64, 1973 (1976); Y. S. Kim and R. G. Gordon, J. Chem. Phys. 61, 1 (1974). Rate coefficients for the formation and dissociation of the similar molecule, KAr^+, have been measured by G. E. Keller, R. A. Beyer and L. M. Colonna-Romano, Phys. Rev. A 8, 1446 (1973).
8. G. York and A. Gallagher, "High Power Gas Lasers Based on Alkali-Dimer A-X Band Radiation," JILA Rept. 114 (1974) Joint Institute for Laboratory Astrophysics, University of Colorado, Boulder, Colorado 80309. For laser operation on the B-X band of Na_2 see B. Welleghausen, S. Shahdin, D. Friede and H. Wellig, Appl. Phys. 13, 97 (1977).
9. J. N. Bardsley, B. R. Junker and D. W. Norcross, Chem. Phys. Lett. 37, 502 (1976).
10. M. A. Biondi, private communication. For a concurrent recognition of the absence of dissociative recombination for asymmetric diatomic molecules

such as HeH^+ see, M. I. Chibisov and S. I. Yakovlenko, Zh. Eksp. Teor. Fiz. 73, 43 (1977) [Sov. Phys.-JETP 46, 21 (1977)].

11. D. E. Nitz, P. B. Hogan, L. D. Schearer and S. J. Smith, J. Phys. B 12, L103 (1979); T. Uzer and A. Dalgarno, Chem. Phys. Letters 61, 213 (1979).
12. W. L. Morgan and A. V. Phelps, private communciation. See also, L. Vriens and F. A. S. Ligthart, Philips Res. Reports 32, 1 (1977).
13. A. V. Phelps, D. Leep and A. Gallagher, Bull. Am. Phys. Soc. 23, 141 (1978). For discussions of simplified models of electron-excited state processes in low density gases see, for example, D. R. Bates, Proc. Roy. Soc. A 337, 15 (1974) and L. M. Biberman, V. S. Vorob'ev and I. T. Yakubov, Usp. Fiz. Nauk. 107, 353 (1972) [Sov. Phys.-Usp. 15, 375 (1973)].
14. J. N. Bardsley and M. A. Biondi, Adv. Atom. Mol. Phys. 6, 1 (1970).
15. Y. Shiu, M. A. Biondi and D. P. Sipler, Phys. Rev. A 15, 494 (1977).
16. Y.-T. Lee and B. H. Mahan, J. Chem. Phys. 42, 2893 (1965). See also A. Klucharev, V. Sepman and Vajnovic, J. Phys. B 10, 715 (1972).
17. M. R. Flannery, Ann. Phys. 61, 464 (1970).
18. T. F. Gallagher and W. E. Cooke, Phys. Rev. A 19, 2161 (1979).
19. A. C. Hindermash, GEAR: Ordinary Differential Equation System Solver, Lawrence Livermore Laboratory Report No. UCID 30001 (1972).
20. L. W. Schumann, D. W. Wildman and A. C. Gallagher, J. Appl. Phys. 50, 7965 (1979).
21. L. S. Frost and A. V. Phelps, Phys. Rev. A 136, 1538 (1964).
22. R. Shuker, A. V. Phelps and A. C. Gallagher, in Electronic Transition Lasers II, edited by L. E. Wilson, S. N. Suchard and J. I. Steinfeld (MIT Press, 1977), p. 208. For details see Final Report for ERDA Contract No. E(49-1)-3800, February 1977 (unpublished).

23. R. F. Boikova and V. D. Obeydkov, Zh. Eksp. Teor. Fiz. 54, 1439 (1968) [Sov. Phys.-JETP 27, 772 (1968)]. See also S-I. Chu and A. Dalgarno, Phys. Rev. A 10, 788 (1974); A. S. Dickinson and J. M. Munoz, J. Phys. B 10, 3151 (1977).

24. S. Geltman, J. Quant. Spectrosc. Radiat. Transfer 13, 601 (1978).

25. S. A. Lawton and A. V. Phelps, J. Chem. Phys. 69, 1055 (1978).

26. R. B. Green et al, IEEE J. Quantum Electron. QE-13, 63 (1977).